High-Performance Analog Products

# Analog Applications Journal

Third Quarter, 2012

## IMPORTANT NOTICE

Texas Instruments Incorporated and its subsidiaries (TI) reserve the right to make corrections, enhancements, improvements and other changes to its semiconductor products and services per JESD46C and to discontinue any product or service per JESD48B. Buyers should obtain the latest relevant information before placing orders and should verify that such information is current and complete. All semiconductor products (also referred to herein as "components") are sold subject to TI's terms and conditions of sale supplied at the time of order acknowledgment.

TI warrants performance of its components to the specifications applicable at the time of sale, in accordance with the warranty in TI's terms and conditions of sale of semiconductor products. Testing and other quality control techniques are used to the extent TI deems necessary to support this warranty. Except where mandated by applicable law, testing of all parameters of each component is not necessarily performed.

TI assumes no liability for applications assistance or the design of Buyers' products. Buyers are responsible for their products and applications using TI components. To minimize the risks associated with Buyers' products and applications, Buyers should provide adequate design and operating safeguards.

TI does not warrant or represent that any license, either express or implied, is granted under any patent right, copyright, mask work right, or other intellectual property right relating to any combination, machine, or process in which TI components or services are used. Information published by TI regarding third-party products or services does not constitute a license to use such products or services or a warranty or endorsement thereof. Use of such information may require a license from a third party under the patents or other intellectual property of the third party, or a license from TI under the patents or other intellectual property of TI.

Reproduction of significant portions of TI information in TI data books or data sheets is permissible only if reproduction is without alteration and is accompanied by all associated warranties, conditions, limitations, and notices. TI is not responsible or liable for such altered documentation. Information of third parties may be subject to additional restrictions.

Resale of TI components or services with statements different from or beyond the parameters stated by TI for that component or service voids all express and any implied warranties for the associated TI component or service and is an unfair and deceptive business practice. TI is not responsible or liable for any such statements.

Buyer acknowledges and agrees that it is solely responsible for compliance with all legal, regulatory and safety-related requirements concerning its products, and any use of TI components in its applications, notwithstanding any applications-related information or support that may be provided by TI. Buyer represents and agrees that it has all the necessary expertise to create and implement safeguards which anticipate dangerous consequences of failures, monitor failures and their consequences, lessen the likelihood of failures that might cause harm and take appropriate remedial actions. Buyer will fully indemnify TI and its representatives against any damages arising out of the use of any TI components in safety-critical applications.

In some cases, TI components may be promoted specifically to facilitate safety-related applications. With such components, TI's goal is to help enable customers to design and create their own end-product solutions that meet applicable functional safety standards and requirements. Nonetheless, such components are subject to these terms.

No TI components are authorized for use in FDA Class III (or similar life-critical medical equipment) unless authorized officers of the parties have executed a special agreement specifically governing such use.

Only those TI components which TI has specifically designated as military grade or "enhanced plastic" are designed and intended for use in military/aerospace applications or environments. Buyer acknowledges and agrees that any military or aerospace use of TI components which have not been so designated is solely at the Buyer's risk, and that Buyer is solely responsible for compliance with all legal and regulatory requirements in connection with such use.

TI has specifically designated certain components which meet ISO/TS16949 requirements, mainly for automotive use. Components which have not been so designated are neither designed nor intended for automotive use; and TI will not be responsible for any failure of such components to meet such requirements.

| **Products** | |
|---|---|
| Audio | www.ti.com/audio |
| Amplifiers | amplifier.ti.com |
| Data Converters | dataconverter.ti.com |
| DLP® Products | www.dlp.com |
| DSP | dsp.ti.com |
| Clocks and Timers | www.ti.com/clocks |
| Interface | interface.ti.com |
| Logic | logic.ti.com |
| Power Management | power.ti.com |
| Microcontrollers | microcontroller.ti.com |
| RFID | www.ti-rfid.com |
| OMAP™ Mobile Processors | www.ti.com/omap |
| Wireless Connectivity | www.ti.com/wirelessconnectivity |

| **Applications** | |
|---|---|
| Automotive and Transportation | www.ti.com/automotive |
| Communications and Telecom | www.ti.com/communications |
| Computers and Peripherals | www.ti.com/computers |
| Consumer Electronics | www.ti.com/consumer-apps |
| Energy and Lighting | www.ti.com/energy |
| Industrial | www.ti.com/industrial |
| Medical | www.ti.com/medical |
| Security | www.ti.com/security |
| Space, Avionics and Defense | www.ti.com/space-avionics-defense |
| Video and Imaging | www.ti.com/video |
| **TI E2E™ Community** | **e2e.ti.com** |

Mailing Address: Texas Instruments, Post Office Box 655303, Dallas, Texas 75265

**SSZZ022D**

# Contents



**To view past issues of the**
***Analog Applications Journal*, visit the Web site**
**www.ti.com/aaj**

# Introduction

*Analog Applications Journal* is a collection of analog application articles designed to give readers a basic understanding of TI products and to provide simple but practical examples for typical applications. Written not only for design engineers but also for engineering managers, technicians, system designers and marketing and sales personnel, the book emphasizes general application concepts over lengthy mathematical analyses.

These applications are not intended as "how-to" instructions for specific circuits but as examples of how devices could be used to solve specific design requirements. Readers will find tutorial information as well as practical engineering solutions on components from the following categories:

- Data Acquisition
- Power Management
- Interface (Data Transmission)
- Amplifiers: Audio
- Amplifiers: Op Amps
- Low-Power RF
- General Interest

Where applicable, readers will also find software routines and program structures. Finally, *Analog Applications Journal* includes helpful hints and rules of thumb to guide readers in preparing for their design.

# Easy solar-panel maximum-power-point tracking for pulsed-load applications

**By Chris Glaser**
*Applications Engineer*

## Introduction

Many solar-panel-powered applications need only pulses of power to operate. Systems for data collection or measurement sampling frequently need to turn on, perform a measurement or some other task, transmit the processed or measured data, and return to sleep. In many cases, wirelessly transmitting the data consumes the largest portion of output power. These required power pulses, either for the system itself or for transmitting data, typically are difficult to support with a power-limited supply such as a solar panel. By operating at the solar panel's maximum power point (MPP) and by intelligently drawing the power from the panel, energy can be successfully harnessed to power a pulsed load. This article presents a simple and cost-effective solution for maximum-power-point tracking (MPPT) for use in such pulsed-load systems.

**Figure 1. Graph of a solar panel's MPP**

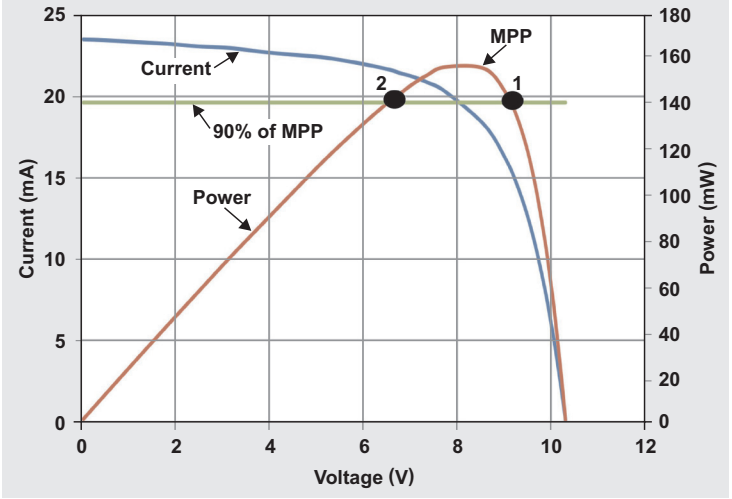


## Solar-panel characteristics

Solar panels provide peak output power when operated at their MPP. The MPP is a voltage and current corresponding to the panel's highest obtainable output power. MPPT harnesses this power from a solar panel even as the amount of illumination varies. A characteristic of solar panels is that the panel voltage decreases as the current drawn from the panel increases. If the current drawn is too high, the voltage collapses and the amount of power drawn becomes very low. Figure 1 illustrates a particular solar panel's output current and output power versus its output voltage. The MPP is labeled. A horizontal green line on the graph shows where the output power is at least 90% of the MPP. Above this line, between Points 1 and 2, the panel provides the most power.

When the solar-panel-powered load requires only pulses of power and does not need to be powered 100% of the time, one simple way to operate within 90% of the MPP is to turn on the load at Point 1 and turn it off at Point 2. When the load is on, it draws its required power, which lowers the panel voltage. This moves the operating point from Point 1, through the MPP point, and over to Point 2. At Point 2, the load is turned off and the panel voltage rises again. Even with this simple operation, there are three issues that must be overcome.

First, the load likely requires a different voltage than what the panel outputs. Thus, a high-efficiency power supply is required to convert the variable and relatively high panel voltage into a constant voltage for the load.

Second, the panel voltage should be measured and the power supply disabled or enabled based on that voltage. Most power supplies have a digital input to enable or disable them. Such an input has a very imprecise threshold to differentiate a logic low from a logic high. With an imprecise threshold, the panel voltage cannot be wired directly to the enable input. Instead, an external circuit with a precise threshold is required. A supply-voltage supervisor can be used, but this adds the cost and complexity of a second device.

Third, the quickly changing panel voltage must be greatly slowed down to allow sufficient operating time to accomplish the required tasks. Changing the panel voltage from Point 1 to Point 2 requires almost no time—theoretically zero seconds. During this time, when the voltage varies from Point 1 to Point 2, the power supply for the load must turn on and the load must perform its task. This requires a power supply with a very fast turn-on and a long enough holdup of the panel voltage to perform the necessary tasks.

## The MPPT solution

There are few single-device, cost-effective solutions that operate from the wide voltage range of power-limited solar-panel inputs while efficiently providing a regulated output voltage, a quick start-up, and operation within 90% of the MPP. However, the Texas Instruments TPS62125 is

one such device that accepts input voltages of up to 17 V, operates with efficiencies in excess of 90%, starts up in less than 1 ms, and has an enable input pin with a precise threshold that can be directly wired to the solar panel's voltage for MPPT. This eliminates the need for an additional device to perform this function. Figure 2 shows a complete solution.

**Figure 2. MPPT circuit for a pulsed load**

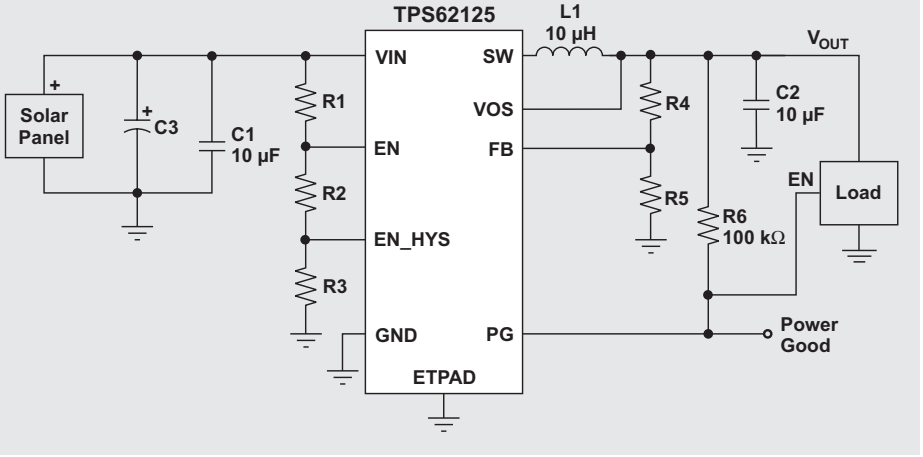


The voltage divider, formed by R1 and R2, is configured to turn on the power supply at Point 1 in Figure 1. Until the power supply is enabled, the device itself holds the node between R2 and R3 at ground potential. After the supply is enabled, the device releases this node, and R3 is then part of the voltage divider. When the solar-panel voltage falls to Point 2, the device turns off and holds the node low between R2 and R3 again. At this point, the panel voltage begins to rise again until it reaches the turn-on threshold. This provides a fully programmable turn-on and turn-off voltage that can be configured to any solar panel.

The bulk input capacitor, C3, stores enough energy from the solar panel to power the load for the required duration and provides the charge for starting up the power supply. The panel delivers a current corresponding to its voltage to either the power supply or C3. When the power supply is off, the solar panel delivers its current to the capacitor. When the power supply is on, the capacitor and solar panel provide the necessary current to power the load. Since C3 merely stores energy and this energy is released over a relatively lengthy period of time, C3 can be a low-cost electrolytic capacitor.

## Computing the required bulk input capacitance

The first step in designing the MPPT circuit is determining the load's power needs and then computing the amount of required bulk input capacitance based on these power requirements and the chosen solar panel. As an example, assume a remote sensing circuit requires 3.3 V at 250 mA (825 mW) for a duration of 15 ms. These are typical needs for a system that contains a measurement device, a microprocessor, and an RF transmitter.

After the load's power needs are determined, the required value for C3 is calculated. First, the input current required to power the load is found from Equation 1:

$$I_{IN} = \frac{\text{Output Power}}{V_{IN} \times \eta} \quad (1)$$

$V_{IN}$ is the average solar-panel voltage between Points 1 and 2 in Figure 1, and $\eta$ is the power-supply efficiency at the given output power. Notice that the typical efficiency of the power supply at a $V_{IN}$ of about 7.8 V and an output power of 825 mW is around 87%. Using these numbers, $I_{IN}$ = 122 mA. This is much greater than what Figure 1 shows the solar panel to be capable of providing, so C3 must store enough energy to provide the remaining current for 15 ms. Equation 2 determines the required C3 value based on the load requirements and solar-panel characteristics:

$$C3 \geq \frac{(I_{IN} - I_{Panel(Avg)}) \times t_{ON}}{V_{P1} - V_{P2}} \quad (2)$$

$V_{P1}$ and $V_{P2}$ are the voltages at Points 1 and 2, which are respectively about 9 V and 6.5 V for this panel, and correspond to the voltage change across C3 as it discharges. The required load operating time, given by $t_{ON}$, is 15 ms. Finally, $I_{Panel(Avg)}$ is the average current from the solar panel when the panel is operated within 90% of its MPP. As seen in Figure 1, this current is about 19 mA.

From Equation 2, it is determined that C3 should be greater than 618 µF. A 680-µF capacitor is used to provide some margin in the operating time.

## Calculating the enable pin's voltage divider

R1, R2, and R3 form a fully configurable voltage divider with hysteresis for the enable (EN) pin. Equations 3 and 4 are used to set the resistor values:

$$V_{P1} = 1.20\ V \times \left(\frac{R1}{R2} + 1\right) \quad (3)$$

$$V_{P2} = 1.15\ V \times \left(\frac{R1}{R2 + R3} + 1\right) \quad (4)$$

R1 is chosen first, and 1 MΩ is a good starting value. With this, R2 is calculated to be 153.8 kΩ. The closest standard value of 154 kΩ is chosen. R3 should be 60.9 kΩ, and 60.4 kΩ is the nearest standard value.

## Additional MPPT circuit configuration

Another feature that can be configured to benefit the typical application is using the power good (PG) output to control the load's enable (EN) input. The PG pin is held low when the power supply is off. The pull-up resistor, R6, pulls it high, but only when the power supply is enabled and the output voltage is in regulation. Connecting the PG output directly to the load's EN input keeps the load disabled until the input voltage has risen above $V_{P1}$ and until the output voltage is high enough to properly power the load. As the power supply is disabled from the input voltage falling below $V_{P2}$, the PG pin is actively pulled low, which also disables the load. This configuration ensures that the load is enabled only when its supply voltage is in regulation, avoiding a low supply voltage that possibly could corrupt the load's performance or data.

## Test results

Figure 3 shows the MPPT circuit in operation. The panel voltage, $V_{IN}$, remains between 9 V and 6.5 V ($V_{P1}$ and $V_{P2}$, respectively). Once $V_{OUT}$ enters regulation, the load enables and draws 250 mA. When the panel's voltage drops to 6.5 V, $V_{OUT}$ is disabled and thereby disables the load current. The solar panel provides an average of 19 mA at all times. The load has a run time of around 18 ms in Figure 3, meeting the 15-ms requirement. This run time roughly matches the calculations, since the value of C3 increased above the result of those calculations.

Figure 4 replaces the output-voltage trace in Figure 3 with the trace for $I_{Cap}$, the current from C3. As $V_{IN}$ decreases, the current leaving the capacitor is positive—the capacitor provides its stored energy to the power supply, which then supplies that energy to the load. Once the load turns off, due to the panel voltage decreasing to 6.5 V and the power supply disabling, the current from C3 goes negative—the capacitor recharges from the panel and stores energy for the next cycle. The current from C3 spikes briefly before the load is enabled, as the power supply turns on when the panel voltage is sufficiently high. Additional input current provided by C3 is needed during start-up.

## Conclusion

This article has demonstrated a simple and cost-effective circuit for tracking a solar panel's MPP for a pulsed-load system, such as a remote measurement system that transmits its data via RF transmitters. This topology also can be configured to any solar panel and any pulsed load.

**Figure 3. Operation of MPPT circuit within 90% of MPP**

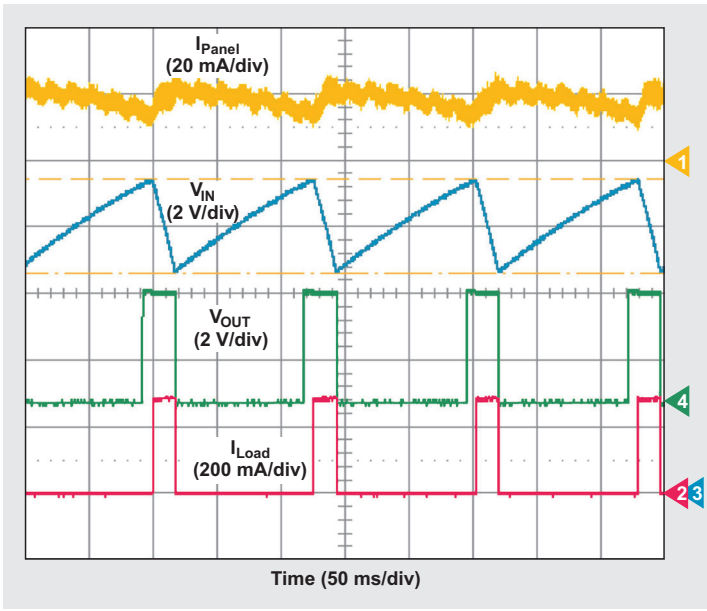


**Figure 4. Bulk input capacitor (C3) supplying a circuit operating within 90% of MPP**

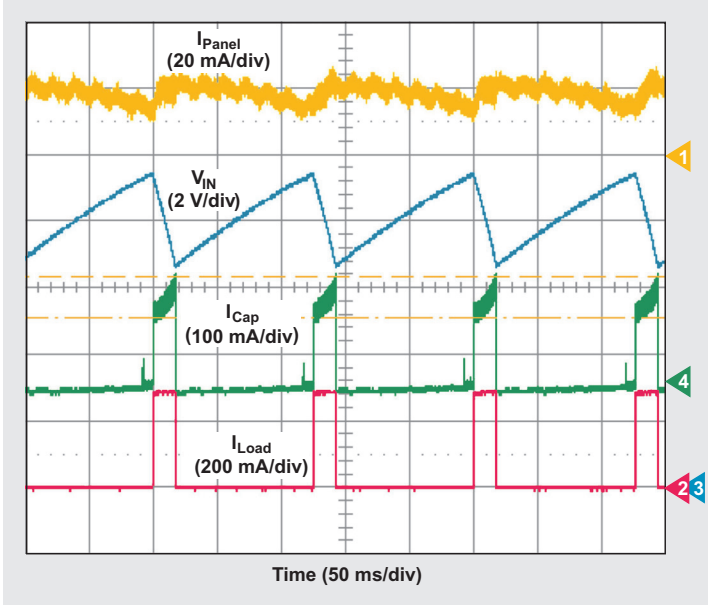


## Related Web sites

**power.ti.com**
**www.ti.com/energyharvesting**
**www.ti.com/product/TPS62125**

# Designing a Qi-compliant receiver coil for wireless power systems, Part 1

**By Bill Johns,** *Applications Engineer,*
**Tony Antonacci,** *System Engineer,*
**and Kalyan Siddabattula,** *System Engineer*

## Overview

The implementation of the Wireless Power Consortium's (WPC's) Qi standard[1] brings wireless power to many different end applications. The receiver (Rx) coil for each application may have different geometries and/or power requirements. Since the Rx coil is a key component in a successful and efficient design of a Qi-compliant Rx and there are many design options and trade-offs to consider, the designer must take a careful and methodical approach when realizing a solution. This article provides the technical insight needed to realize a successful Rx-coil design. It covers the Qi-compliant system model as a basic transformer; Rx-coil measurements and system-level influences; and methods of qualifying a design for successful operation. It is assumed that the reader has a general understanding of the Qi-compliant inductive power system. Background information can be found in Reference 2.

## Qi-compliant system as a transformer

For many near-field wireless power systems such as the one specified by the WPC, the behavior of the magnetic power transfer can be modeled by a simple transformer. A traditional transformer usually has a single physical structure with two windings around a core material that is highly permeable compared to air (Figure 1). Since the traditional transformer uses a highly permeable material to carry the magnetic flux, most (not all) of the flux produced by one coil couples to the second coil. This coupling, which can be measured through a parameter known as the coupling coefficient, is denoted as k (a measure that can have a value between 0 and 1).

Three parameters define a two-coil transformer:

$L_{11}$ is the self-inductance of coil 1.

$L_{22}$ is the self-inductance of coil 2.

$L_{12}$ is the mutual inductance of coils 1 and 2.

The coefficient for coupling between the two coils can be formulated as

$$k = \frac{L_{12}}{\sqrt{L_{11}L_{22}}}. \quad (1)$$

The ideal transformer then can be modeled by using a coupled inductor as shown in Figure 2.

Using the voltage and current relationship of an inductor can provide the nodal equations of this two-coil transformer:

$$V_1 = L_{11}\frac{di_1}{dt} + L_{12}\frac{di_2}{dt} \quad (2a)$$

**Figure 1. Traditional transformer with one physical structure**

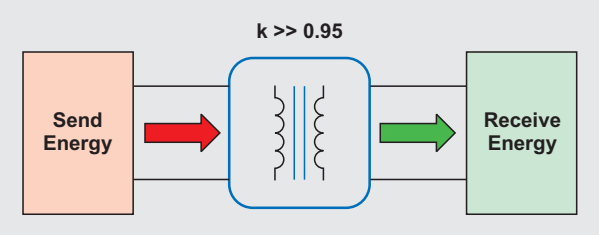


**Figure 2. Ideal model of a traditional transformer**

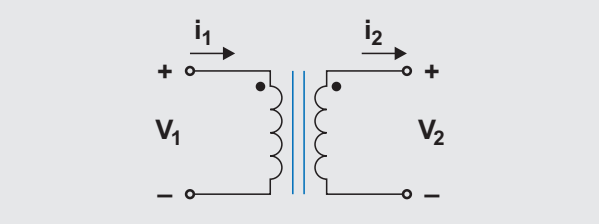


**Figure 3. Cantilever model of a traditional transformer**

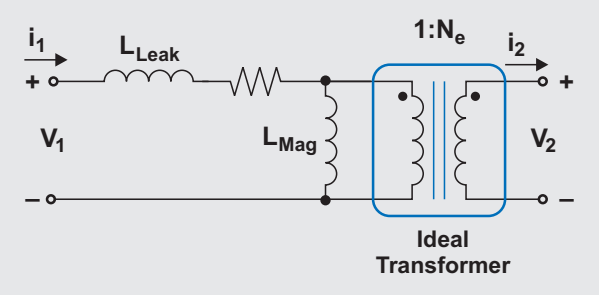


$$V_2 = L_{22}\frac{di_2}{dt} + L_{12}\frac{di_1}{dt} \quad (2b)$$

For circuit analysis, the model in Figure 2 can be represented by what traditionally is referred to as a cantilever model, shown in Figure 3. Here the magnetic coupling and mutual inductance are simplified to leakage and magnetizing inductances. This allows the physical nature of the

coupling to be understood through a circuit implementation. For the ideal transformer, the turns ratio is calculated by using the following equations:

$$N_e = \frac{1}{k}\sqrt{\frac{L_{22}}{L_{11}}} \quad \textbf{(3a)}$$

$$L_{Mag} = k^2 L_{11} \quad \textbf{(3b)}$$

In a tightly coupled system, the leakage inductance is a small percentage of the magnetizing inductance, allowing this parameter to be neglected for a first-order approximation. In addition to high coupling, the series resonant capacitors utilized in the Qi-compliant system reduce the effect of leakage inductance. Therefore, the voltage gain from the primary coil to the secondary coil can be approximated for the first order as

$$\frac{V_2}{V_1} \propto k\sqrt{\frac{L_{22}}{L_{11}}}. \quad \textbf{(4)}$$

The transformer in a Qi-compliant system consists of two separate physical devices, the transmitter (Tx) and the receiver (Rx), each with an isolated coil. When a Tx and Rx are placed near one another, they form a coupled-inductor relationship, simply modeled as a two-coil transformer with an air core (Figure 4). The shielding material on both sides serves as a magnetic-flux short. This allows the magnetic field lines (flux) to be contained between the two coils. Figure 5 illustrates a 2D simulation of the magnetic field lines found during typical operation.

For a typical Qi-compliant system, the coupling coefficient (k) is much lower than for a traditional transformer. A traditional transformer has coupling in the range of 0.95 to 0.99. For example, 95 to 99% of the magnetic flux couples to the secondary coil; whereas, for a Qi-compliant system, the coupling coefficient is on the order of 0.2 to 0.7, or 20 to 70%. For the most part, the Qi standard attempts to mitigate this lower coupling with a series resonant cap on the Tx and Rx that can compensate for the leakage inductance at resonance.

## Electrical requirements of the Rx coil

In some Rx ICs, the target voltage of the dynamically controlled rectifier varies as a function of the output current. Since the rectifier output dictates the voltage gain needed across the transformer, the highest output voltage on the rectifier must be considered along with the output load, or demand for output power. As shown in Figure 6, the rectifier output varies from ~7 to 5 V over a 1-A load, which sets the required voltage gain across the transformer. It is important to ensure that the Rx coil, when tuned per the WPC specification (see the section "Tuning the Rx coil" later in this article), can achieve this voltage demanded by the Rx IC.

**Figure 4. Simple inductively coupled transformer with an air core**

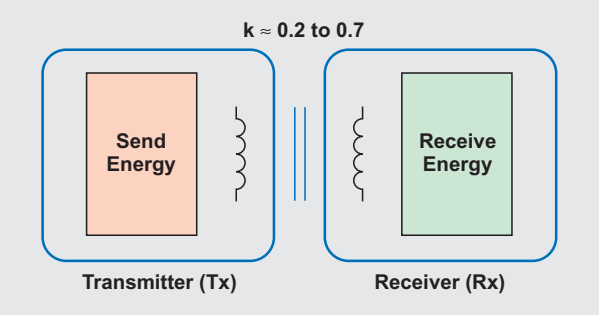


**Figure 5. Example magnetic field lines between two mutually coupled coils**

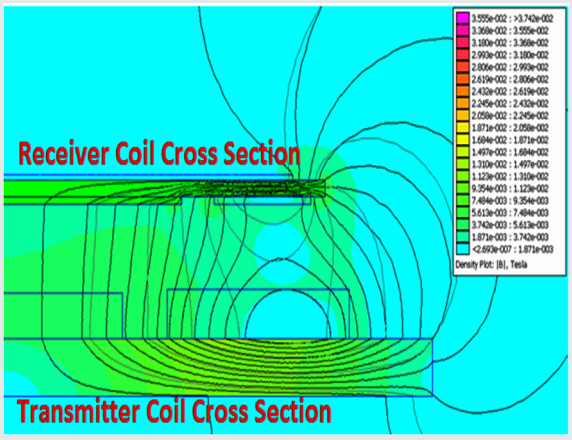


**Figure 6. Rectifier output versus load**

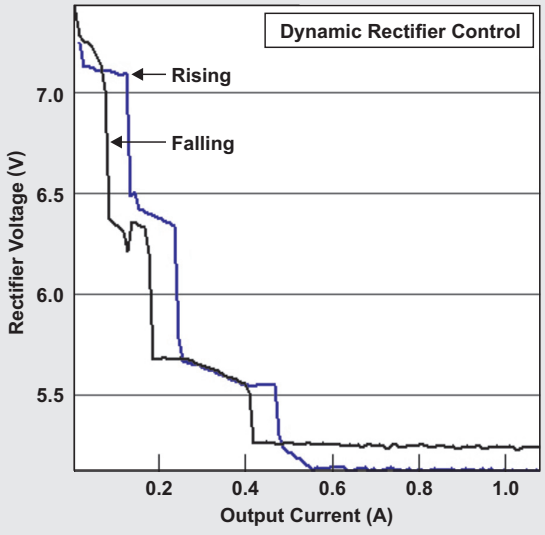

The flowchart in Figure 7 illustrates a recommended approach for specifying a new Rx coil. The design flow has limited choices for the shield, the wire gauge, and the number of turns. Each of these will be discussed next.

### The shield

The shield has two primary functions: (1) providing a low-impedance path for the magnetic flux so that very few flux lines impinge upon surrounding metallic objects, and (2) permitting a higher-inductance coil to be realized with fewer turns so that excessive resistance is not introduced (from additional turns).

Thick shields, which can absorb a large amount of magnetic flux (i.e., they have a high flux saturation point), can be used to prevent heating in the material behind the Rx coil. Thick shields also are less susceptible to drops in efficiency than thinner shields when they encounter a Tx or Rx with a magnet used for alignment. (See the section "Measuring the Rx-coil inductance" later in this article for details on this effect.) Typical materials from vendors such as Vishay, TDK, Panasonic, E&E, Elytone, and Mingstar can help minimize efficiency degradation. Note that high-permeability ferrite materials, such as powdered iron, don't always perform better than distributed-gap materials. Although ferrite materials have a high permeability, they exhibit a lower flux saturation point when the shield thickness is reduced. This factor must be carefully considered.

### The Rx-coil wire gauge

The choice of wire gauge for the Rx coil is based on cost versus performance. Large-diameter wire or bifilar wire (two parallel wires) can provide high efficiencies but is costly and can result in thick Rx-coil designs. For instance, a PCB coil might be cheaper in overall cost but incurs a much higher equivalent series resistance than a bifilar counterpart.

### The number of turns

Once the wire and shield have been chosen, the number of turns determines the Rx-coil inductance. Coil inductance and coupling determine the voltage gain observed at the Rx's rectifier output as well as the total available power to the Rx. This voltage-gain target is shown in Figure 6.

Three procedures offer a general approach to determine the inductance target:

1. The Tx's type-A1 coil should be used as the basis for the primary coil's characteristics (for example, 1500-mm$^2$ area, 24-µH inductance, and 19-V primary voltage).
2. When a shield material with a permeability significantly higher than air (>20) is used, the coil area is a good proxy for the coupling coefficient. Note that this only applies to planar coils with either a single layer or two layers of turns. Exotic coil structures do not utilize this principle. In order to ensure a reasonable coupling and high efficiency, an Rx coil can be used with an area approximately 70 to 80% of the area of A1 coil for a 5-W system. This ensures a coupling coefficient of approximately 50% for most reasonable designs with a distance, $d_Z$, of up to 5 mm between the Tx and Rx coils as specified by the WPC.
3. The desired voltage gain is determined based on the average expected rectifier voltage—for example, 6 V found in the plot in Figure 6. In this example case, the voltage gain is ~0.32 (6 V/19 V).

**Figure 7. Flowchart of methodology for Rx-coil design**

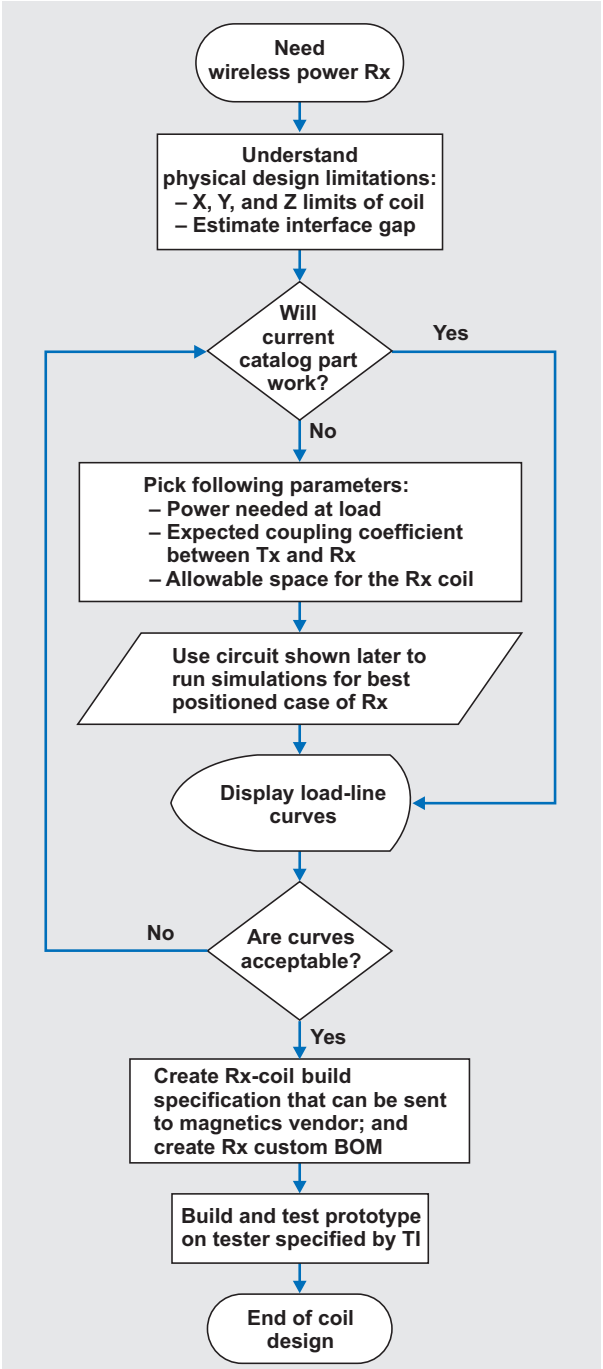

A typical design for a 5-V/5-W output-voltage system shows that with the coupling coefficient around 0.5, a secondary inductance of about 10 µH is sufficient to produce the target voltages required. There are two relationships to consider in the system design:

$$V_2 \propto kV_{IN}\sqrt{\frac{L_{22}}{L_{11}}} \quad \textbf{(5a)}$$

$$L_{22} \propto N_2^2 \quad \textbf{(5b)}$$

Therefore, if the coupling coefficient is changed from 0.5 to 0.4, the inductance for the same power output can increase by up to 1.6 times the previous inductance. This means that the new inductance is ~16 µH. As shown in Equation 5b, coil inductance is proportional to the number of coil turns squared.

Table 1 shows the secondary inductance and coupling for some common coils designed for the system.

**Table 1. Examples of typical coils**

| COIL DIMENSIONS (mm) | TURNS | $V_{OUT}$ (V) | $P_{OUT}$ (W) | $L_{22}$ (µH) | k |
|---|---|---|---|---|---|
| 48 × 32 | 15 | 5 | 5 | 12 | ~0.6 |
| 28 × 14 | 24 | 5 | 2.5 | 33 | ~0.25 |
| 35 × 35 | 24 | 7 | 5 | 22 | ~0.5 |

One caveat is that these rules of thumb apply to general planar coils and are preliminary, meant to serve as a starting point for a design. The actual design is best optimized by using simulation tools, as shown in the flowchart in Figure 7.

## Measuring the Rx-coil inductance

The Rx-coil inductance is a very important parameter that dictates the electrical response (such as voltage gain and output impedance) of the Rx AC/DC power stage. To preserve a consistent response, the inductance must minimally vary in different system scenarios. Due to the interoperability nature of the Qi standard, the Rx coil can be placed on many different types of Tx's that may influence the Rx-coil inductance—and hence the electrical response.

Per Section 4.2.2.1 of the WPC specification,[1] the Rx-coil inductance, $L'_S$, is measured with the test configuration in Figure 8. The spacer and Tx shield provide a reference to emulate Tx components near the Rx coil. In this test configuration, the Tx shield is a 50 × 50 × 1-mm piece of ferrite material (PC44) from TDK Corporation. The gap $d_Z$ is set to 3.4 mm by means of a nonmetallic spacer. The Rx coil is then placed on the spacer, and $L'_S$ is measured with a stimulus of 1-V RMS and 100 kHz. In addition, the free-space Rx-coil inductance, $L_S$, is measured without the Tx shield.

What is not detailed in the WPC specification is the influence of common system scenarios on the $L'_S$ and $L_S$ measurements. The most common influence on these parameters is the presence of a battery behind the Rx coil. Due to the casing material and the battery cell's makeup, the Rx-coil inductance generally is reduced when the battery is placed behind it. In addition to the battery, the presence of a magnet on a Tx-coil structure influences the inductance. (See Section 3.2.1.1.4 of the WPC specification.[1]) The magnet functions as a stressor on the Rx-coil shielding material where the shield's magnetic saturation point is of key interest. If the Rx-coil shielding material saturates when a magnet is present, the coil inductance drops dramatically. Because the Qi standard specifies Tx coil assemblies with and without a magnet, the designer needs to understand how the inductance varies in both scenarios, as any shift in inductance will shift the resonant tuning of the Rx. Note that the test configuration in Figure 8 does not include a magnet. When a magnet is included, its flux density should be between 75 and 150 mT and its diameter should be a maximum of 15.5 mm. This means that the typical 30-mT magnetic field of the Tx coil during power transfer is about 20% of the magnet's field strength.

**Figure 8. Test configuration for measuring Rx-coil inductance ($L'_S$)**

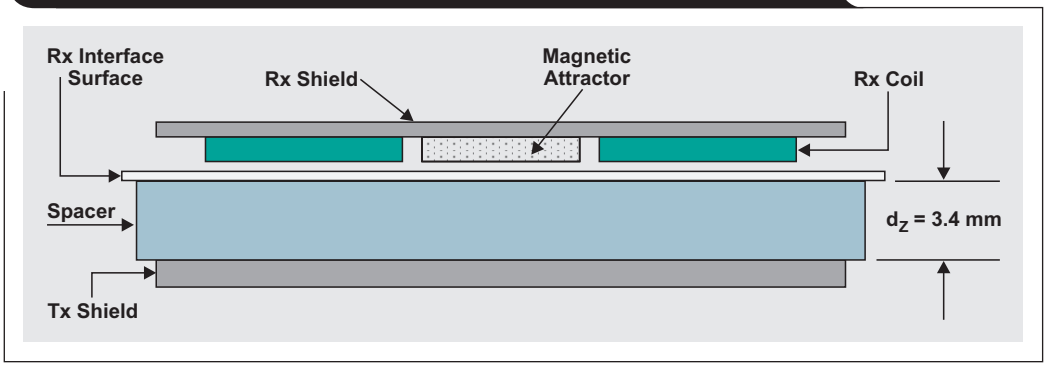

**Table 2. Rx-coil-inductance parameters to be measured during development**

| PARAMETER | Rx COIL WITH Tx SHIELD | Rx COIL WITHOUT Tx SHIELD | BATTERY | MAGNET | SUMMARY |
|---|---|---|---|---|---|
| $L'_S$ | Included | — | — | — | Standard $L'_S$ measurement |
| $L'_S$_m | Included | — | — | Included | Exposes the effect of the magnet |
| $L'_S$_b | Included | — | Included | — | Exposes the effect of the battery |
| $L'_S$_m_b | Included | — | Included | Included | Exposes the effect of the battery and the magnet together |
| $L_S$ | — | Included | — | — | Standard $L_S$ measurement |
| $L_S$_b | — | Included | Included | — | Exposes the effect of the battery |

For the purpose of understanding the performance of the Rx-coil inductance, Table 2 defines parameters in addition to the recommended measurements of $L'_S$ and $L_S$. When the battery is introduced into the measurement, it should be placed in the same orientation/location as it will be in the final system. Note that the materials used in the final industrial design could also influence the final inductance measurement. Therefore, when the tuning circuit is configured, all components of the final industrial design of the mobile device should be used for the final measurement. The measurements found in Table 1 can be used to screen and qualify potential Rx coils.

Table 3 summarizes the measured inductances from an acceptable coil design and the resonant frequency with a fixed series and parallel resonant capacitor. Here $L'_S$_b was used for the capacitor calculations. (See the next section, "Tuning the Rx coil," for details.) Note that the variation could be linearly scaled as a percentage of $L'_S$ and used as a reference for acceptance of a prototype coil.

**Table 3. Measured inductances of a sample coil**

| | $L'_S$ | $L'_S$_m | $L'_S$_b | $L'_S$_m_b | $L_S$ | $L_S$_b |
|---|---|---|---|---|---|---|
| Inductance (μH) | 12.9 | 13.1 | 10.5 | 10.6 | 10.9 | 9.52 |
| Resonance (kHz) | 90.15 | 89.63 | 100 | 99.72 | 98.15 | 105.02 |

## Tuning the Rx coil

The simplified Rx-coil network consists of a series resonant capacitor, $C_1$, and a parallel resonant capacitor, $C_2$. These two capacitors make up the dual resonant circuit with the Rx coil (see Figure 9) and must be sized correctly per the WPC specification.

To calculate $C_1$, the resonant frequency of 100 kHz is used along with $L'_S$:

$$C_1 = \frac{1}{(100\ \text{kHz} \times 2\pi)^2 \times L'_S} \quad (6)$$

To calculate $C_2$, a secondary resonance of 1.0 MHz is used along with $L_S$. This calculation requires that $C_1$ be determined first and used in Equation 7:

$$C_2 = \frac{1}{(1.0\ \text{MHz} \times 2\pi)^2 \times \left(L_S - \frac{1}{C_1}\right)} \quad (7)$$

Finally, the quality factor must be greater than 77 and is calculated as

$$Q = \frac{2\pi \times 1.0\ \text{MHz} \times L_S}{R}, \quad (8)$$

where R is the DC resistance of the coil.

## Load-line analysis of the Rx coil

When choosing an Rx coil, a designer needs to understand the transformer characteristics by comparing the primary and Rx coils via load-line analysis (I-V curves). This analysis captures two important conditions in the Qi-compliant system: (1) operating-point characteristics and (2) transient response. These will be discussed next.

**Figure 9. Dual resonant circuit with Rx coil**

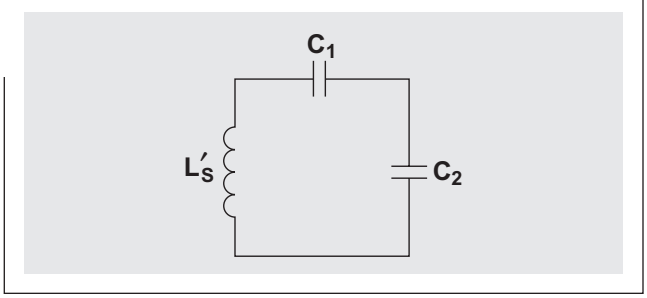

### Operating-point characteristics

An example test configuration for conducting load-line analysis is shown in Figure 10, whose parameters are defined as follows:

$V_{IN}$ is an AC power source that should have a peak-to-peak operation of 19 V.

$C_P$ is the primary series-resonant capacitor (100 nF for type-A1 coil).

$L_P$ is the primary coil of interest (type A1).

$L_S$ is the secondary coil of interest.

$C_1$ is the series resonant capacitor chosen for the Rx coil under test.

$C_2$ is the parallel resonant capacitor chosen for the Rx coil under test.

$C_B$ is the bulk capacitor for the diode bridge. $C_B$ should be at least 10 µF at 25 V.

V is a Kelvin-connected voltage meter.

A is a series ammeter.

$R_L$ is the load of interest.

The diode bridge should be constructed of Schottky diodes in either a full bridge or a synchronous half bridge with low-side n-type MOSFETs and high-side Schottkys. Three test procedures are used for the analysis:

**Figure 10. Test setup for load-line analysis**

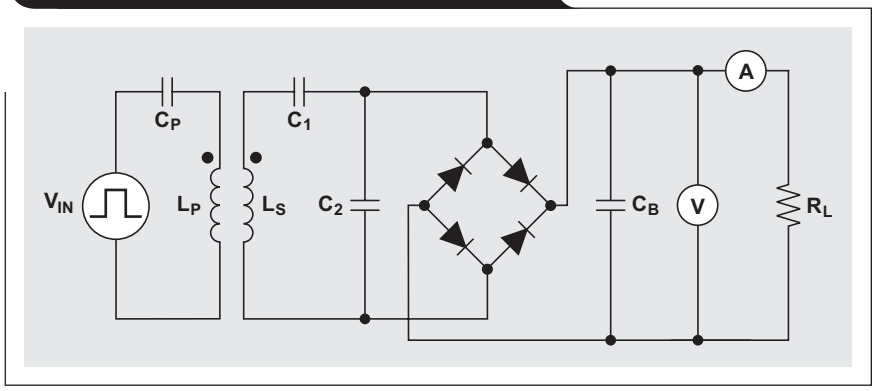


1. A 19-V AC signal is supplied to $L_P$, starting at a frequency of 200 kHz.
2. The resulting rectified voltage is measured from no load to the expected full load.
3. The preceding two steps are repeated for lower frequencies, stopping at 110 kHz.

An example load-line analysis is shown in Figure 11. The plot conveys that specific load and rectifier conditions result in a specific operating frequency. For example, at

**Figure 11. Results of example load-line analysis**

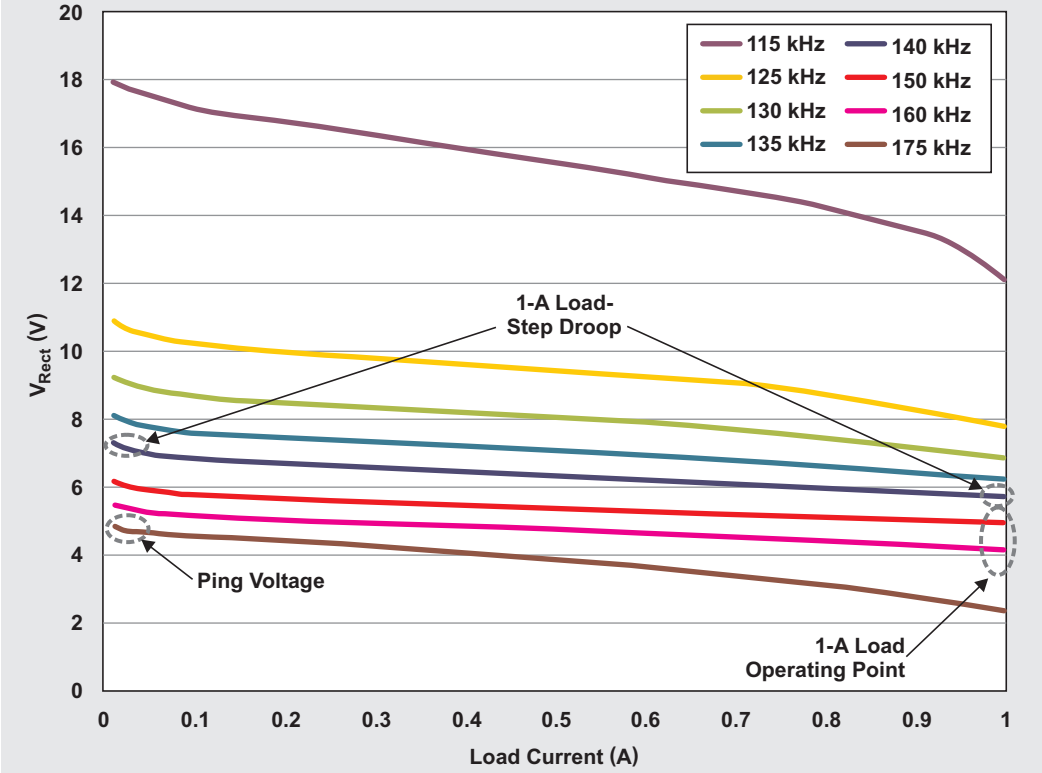

1 A, the target for the dynamic rectifier is 5.15 V. Therefore, the operating frequency is between 150 and 160 kHz, which is an acceptable operating point. If the operating point falls outside the WPC-specified frequency range of 110 to 205 kHz, the system will never converge and will become unstable.

### Transient response

For transient analysis, there are two major points of interest, shown in Figure 11: (1) the rectifier voltage at the ping frequency (175 kHz), and (2) the rectifier voltage droop from no load to full load at the constant operating point.

In this example, the ping voltage is ~5 V. This is above the $V_{UVLO}$ of the chip. Therefore, start-up in the Qi-compliant system can be guaranteed. If the voltage is near or below the $V_{UVLO}$ at this frequency, start-up may not occur.

If the maximum load step is 1 A, the droop in this example is ~1 V with a voltage of 6 V at the 140-kHz load line in Figure 11. To analyze the droop, the 140-kHz load line that starts at 7 V at no load is followed to the maximum load current expected. Droop voltage is the difference between the voltages at the ends of the load line. Acceptable full-load voltage at the selected operating frequency should be above 5 V. If it descends below 5 V, the power-supply output also droops to this level. This type of analysis for transient response is necessary due to the Qi-compliant system's slow feedback response. The analysis simulates the step response that would occur if the system did not adjust the operating point of the resonant transformer.

Note that coupling between the primary and secondary coils worsens with Rx-coil misalignment. Therefore, an additional analysis of the load lines at multiple misalignments is recommended to determine where in the planar space the Rx discontinues operation.

## Conclusion

This article has shown that traditional transfer fundamentals can be employed to simplify the design of Rx coils for wireless power systems. However, the nature of interoperability and mobile-device characteristics can impose unique deviations from standard magnetics design practices. Identifying and addressing coil-design details up front increases the probability of greater success on the first pass. The evaluation methods introduced allow specification and characterization of a custom Rx coil in a very methodical approach.

Part 2 of this article series will provide design details of different types of custom Rx coils. The results will exercise the methods and theory presented in Part 1.

## References

For more information related to this article, you can download an Acrobat® Reader® file at www.ti.com/lit/*litnumber* and replace "*litnumber*" with the **TI Lit. #** for the materials listed below.


| **Document Title** | **TI Lit. #** |
|---|---|
| 1. Wireless Power Consortium, "System Description Wireless Power Transfer, Vol. I, Part 1," Version 1.1, March 2012 [Online]. Available: http://www.wirelesspowerconsortium.com/downloads/wireless-power-specification-part-1.html | — |
| 2. Bill Johns, "An introduction to the Wireless Power Consortium standard and TI's compliant solutions," *Analog Applications Journal* (1Q 2011) | SLYT401 |


## Related Web sites

**www.ti.com/bqtesla**
**www.ti.com/product/bq500210**
**www.ti.com/product/bq51013A**

# Data-rate independent half-duplex repeater design for RS-485

**By Thomas Kugelstadt**
*Applications Engineer*

A question frequently posed by engineers is how to design a data-rate independent half-duplex repeater for RS-485 applications. Examples include designing a long-haul network beyond the suggested maximum cable length of 1200 m, adding long stubs to an existing network, or designing a network using a star topology. The data rates applied can vary between systems from 10 kbps up to 200 kbps.

Ground-potential differences (GPDs) between remotely located nodes can assume voltages exceeding the maximum common-mode voltage range of most bus transceivers, making galvanic isolation necessary between the network node electronics and the bus.

In Reference 1, the characteristic for cable length versus data rate suggests that a maximum cable length of 1200 m, or about 4000 ft, should be used (Figure 1). At this length, the resistance of the commonly applied 120-Ω, AWG24 unshielded twisted-pair (UTP) cable approaches the value of the termination resistor and reduces the bus signal swing by half, or 6 dB.

In RS-485 literature, transceiver datasheets often show a full-duplex repeater design for simplicity's sake. In long-haul networks, however, it is undesirable to run a full-duplex cable for thousands of meters because cable and wiring are very expensive.

**Figure 1. Cable length versus data rate**

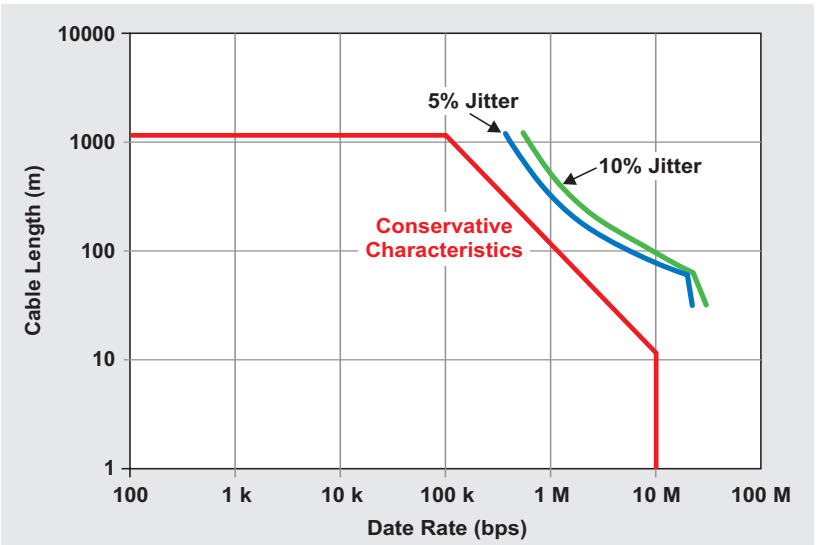


To operate an extended long-haul network in half-duplex mode, implementing a half-duplex repeater is a must. A system block diagram is shown in Figure 2. Because a half-duplex repeater interfaces to two bus segments, the repeater must comprise two separate transceivers, each connecting to its respective bus via signal isolators, and a control logic isolated from both transceiver sections. The control logic performs timely enabling and disabling of the repeater's driver and receiver sections. This is initiated by the incoming data signal from either direction.

**Figure 2. Bus extension with dual isolated half-duplex repeater**

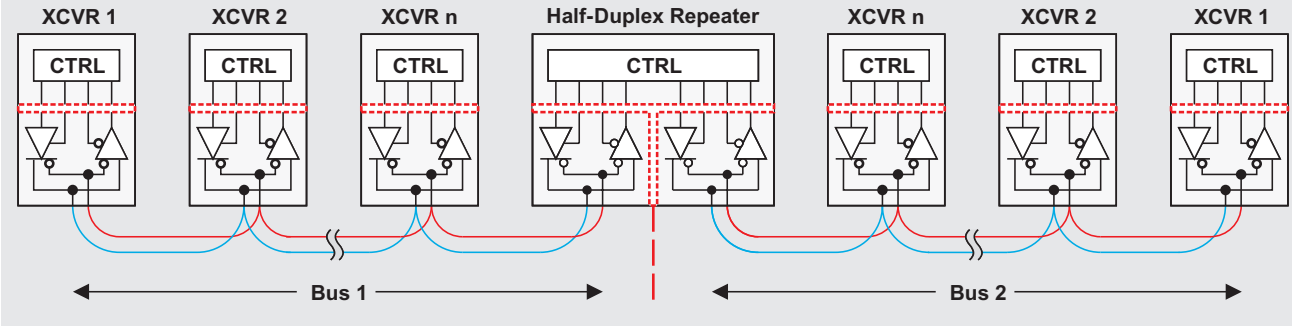

The two most commonly applied timing-control methods are the one-shot circuit in Figure 3 and the inverting buffer with a time delay in Figure 4. To ensure correct switching behavior, both methods require defined start conditions after power up and bus idling. This is accomplished through fail-safe biasing resistors, $R_{FS}$, which create a fail-safe voltage, $V_{FS}$, above the receiver input sensitivity of $V_{FS}$ > +200 mV when no transceiver is actively driving the bus.

A run-through of the one-shot circuit's functional sequence (numbered here and in Figure 3) clarifies the repeater operation:

1. During bus idling, the receiver outputs of both repeater ports are high due to $V_{FS}$. Thus, both transceivers hold each other in receive mode.
2. Next, the arriving start bit of an incoming data packet on port 1 drives the output of $RX_1$ low. This transition triggers the one-shot circuit, driving its output high and enabling driver $DR_2$.
3. The time constant, $R_D \times C_D$, must be so calculated that the one-shot circuit's output remains high for the entire time of the data packet.
4. $DR_2$ continues driving bus 2 for the duration of the one-shot time constant. $XCVR_{OUT}$ represents the receiver output state of a remote transceiver on bus 2. Note that while $DR_2$ is enabled, the pull-up resistor, $R_{PU}$, pulls the disabled receiver's ($RX_2$'s) output high in order to keep $RX_1$ enabled.

A drawback of this solution is that the R-C time constant depends on the data-packet length and the data rate at which the signal is transmitted. Also, one-shot circuits are sensitive to noise transients, which can cause false triggering and repeater breakdown.

**Figure 3. Transceiver timing control with a one-shot circuit**

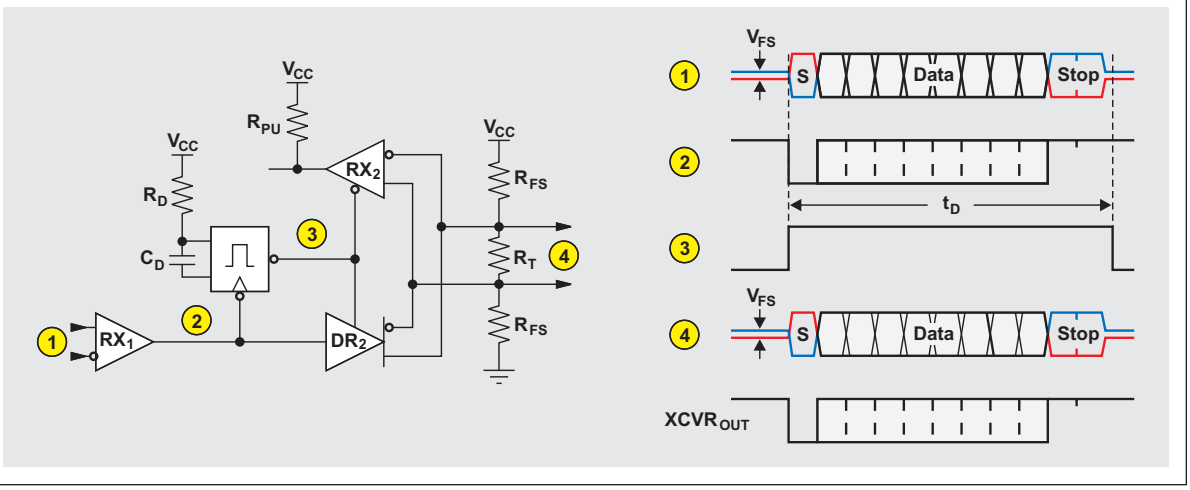


**Figure 4. Transceiver timing control with an inverting buffer**

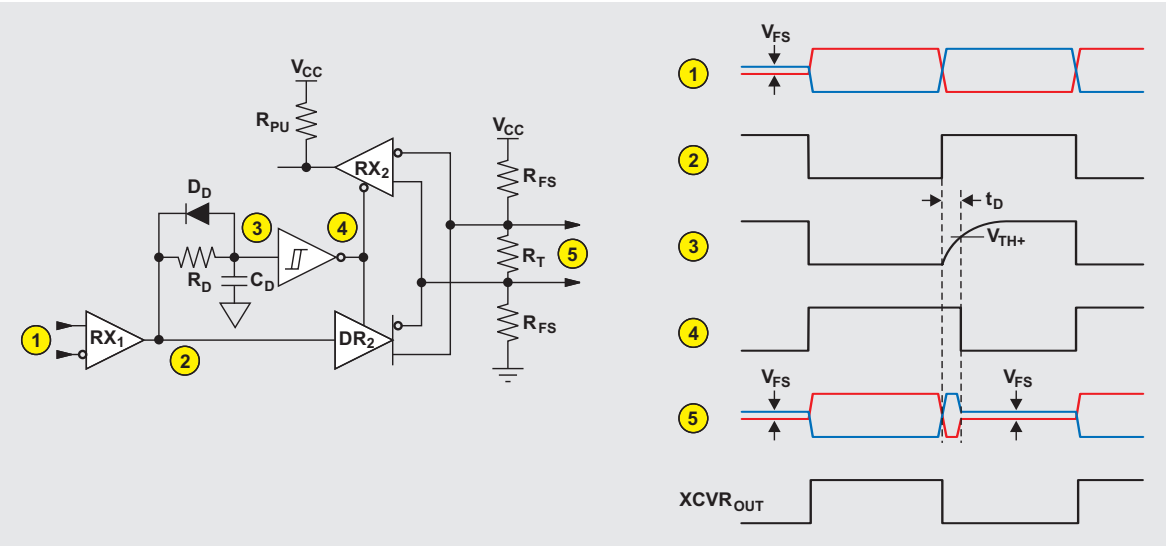

Nevertheless, one-shot circuits are used often in interface bridges such as RS-232 to RS-485 converters. These converters directly connect an RS-485 network to the RS-232 ports of older PCs or RS-232-controlled machinery.

A more robust and data-rate-independent alternative to the one-shot circuit is timing control through an inverting Schmitt-trigger buffer with different charge and discharge times. The underlying principle is to actively drive a bus during logic-low states and to disable the driver during logic-high states. The enabling and disabling sequences then occur on a per-bit basis, which makes the repeater function independent of data rate and packet length.

A run-through of the inverter-controlled repeater's functional sequence (numbered here and in Figure 4) clarifies its operation:

1. During bus idling, the receiver outputs of both repeater ports are high due to $V_{FS}$. The delay capacitor, $C_D$, is fully charged, driving the inverter output low to maintain the transceiver in receive mode.
2. Then a low bit on bus 1, driving the output of $RX_1$ low, rapidly discharges $C_D$ and enables driver $DR_2$.
3. When the bus voltage turns positive ($V_{Bus}$ > 200 mV), the output of $RX_1$ turns high, which drives $DR_2$'s output high and slowly charges $C_D$ via $R_D$. The minimum time constant ($R_D \times C_D$) must be so calculated that at the maximum supply voltage, $V_{CC(max)}$, and the minimum positive inverter input threshold, $V_{TH+(min)}$, the delay time, $t_D$, exceeds the maximum low-to-high propagation delay, $t_{PLH(max)}$, of the driver by, say, 30%. For example, given a capacitance of $C_D$ = 100 pF, the required resistor value for $R_D$ is

$$R_D = \left| \frac{1.3 \times t_{PLH(max)}}{C_D \times \ln\left(1 - V_{TH+(min)} / V_{CC(max)}\right)} \right|.$$

4. The driver enable time is extended by the delay time ($t_D$) versus the actual data-bit interval to establish a valid high signal on the bus. This is done prior to switching from transmit to receive mode in order to keep the receiver output continuously high. Because the propagation delays of receivers are shorter than those of drivers, it is impossible for the receiver to turn low, not even for a short instant. Once the driver is disabled, the external fail-safe resistors bias bus 2 to above 200 mV, which is seen by the active receiver as a defined high.
5. The differential output voltages on bus 2 are $V_{OD} = V_{FS}$ > +200 mV during an idle bus, $V_{OD}$ < 1.5 V for a low bit, and $V_{OD}$ > 1.5 V for the time delay ($t_D$) at the beginning of a high bit. Afterwards, $V_{OD} = V_{FS}$ > +200 mV for the remainder of a high bit.

Again, $XCVR_{OUT}$ represents the receiver output state of a remote transceiver on bus 2. While legacy repeater designs typically were limited to data rates of 10 kbps, modern transceivers with shorter propagation delays allow for higher data rates of up to 100 kbps and more.

For simplicity, the repeater discussion has so far excluded the important aspect of galvanic isolation. However, in long-haul networks—the main application field of repeaters—large ground-potential differences (GPDs) between network nodes are common. These GPDs present themselves as large common-mode voltages across the transceiver inputs and can damage a device if not eliminated through galvanic isolation. When a transceiver's bus circuitry is isolated from its control circuitry, the bus system is floating and independent from a local node's ground potential.

Figure 2 shows the driver and receiver section of a bus node being isolated from the node's control circuitry. However, in the case of the repeater, dual isolation is required because the inner control logic must be isolated from bus 1 and bus 2. Furthermore, the two buses must

be isolated from each other. A repeater circuit accomplishing this is shown in Figure 5, accompanied by its bill of material (BOM) in Table 1. The circuit uses two isolated RS-485 transceivers, each requiring a separate, isolated supply, $V_{ISO}$, derived from the central 3.3-V supply of the control section (Figure 6).

**Table 1. BOM for the repeater's signal path**

| DESIGNATOR | FUNCTION | DEVICE/VALUE | SUPPLIER |
|---|---|---|---|
| U1, U2 | Isolated half-duplex transceiver | ISO15DW | Texas Instruments |
| U3 | Dual Schmitt-trigger inverter | SN74LVC2G14DBV | |
| $R_{PU}$ | Pull-up resistor | 4.7 kΩ | Vishay |
| $R_{FS}$ | Fail-safe resistor | 348 Ω | |
| $R_T$ | Termination resistor | 120 Ω | |
| $R_D$ | Delay resistor | 10 kΩ | |
| $C_S$ | Storage capacitor | 10 µF | |
| $C_B$ | Bypass capacitor | 0.1 µF | |
| $C_D$ | Delay capacitor | 100 pF | |
| $D_D$ | Discharge diode | 1N4448 | |

## Conclusion

A repeater can be used as a bus extender or a stub extender. For a bus extender, a repeater builds the end of one bus and the beginning of another. This allows a fixed installation of fail-safe and termination resistors at both ports. When a repeater is used as an extender for long stubs, however, it can be located anywhere in the network. In this case the resistors at the port side connecting to the bus should be removed, while the resistors at the stub port can remain installed.

## Reference

1. "Application Guidelines for TIA/EIA-485-A," TIA TSB-89, January 1, 2006. Available at www.global.ihs.com

## Related Web sites

**www.ti.com/interface**
**www.ti.com/product/***partnumber*
Replace *partnumber* with ISO15, SN6501, or SN74LVC2G14

**Figure 5. Dual isolated half-duplex repeater**

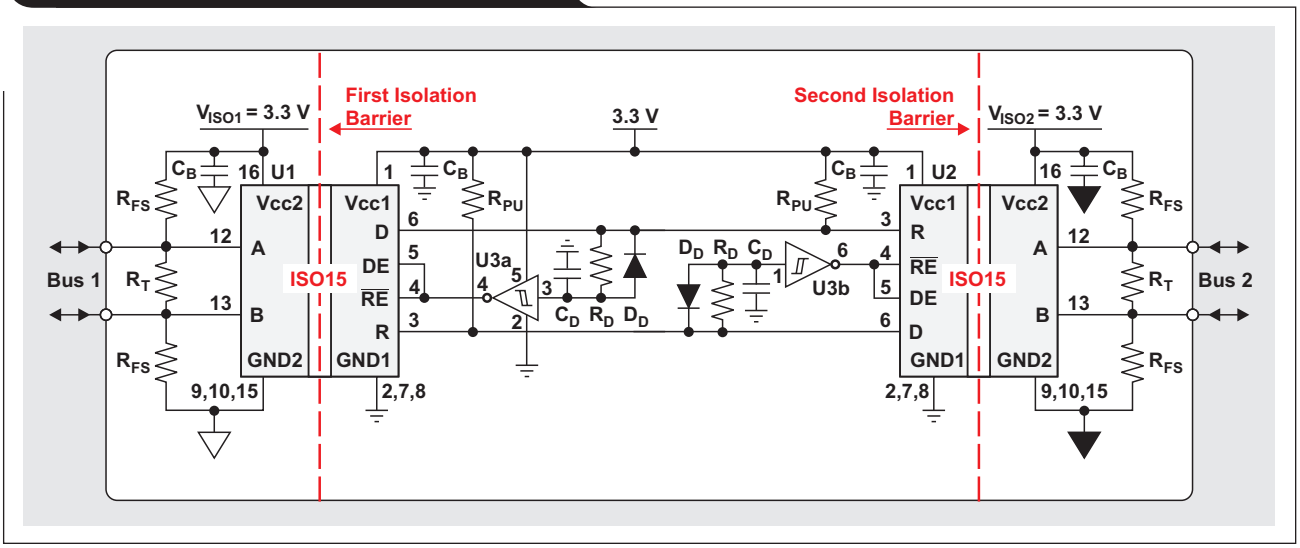


**Figure 6. Design for dual isolated power supplies**

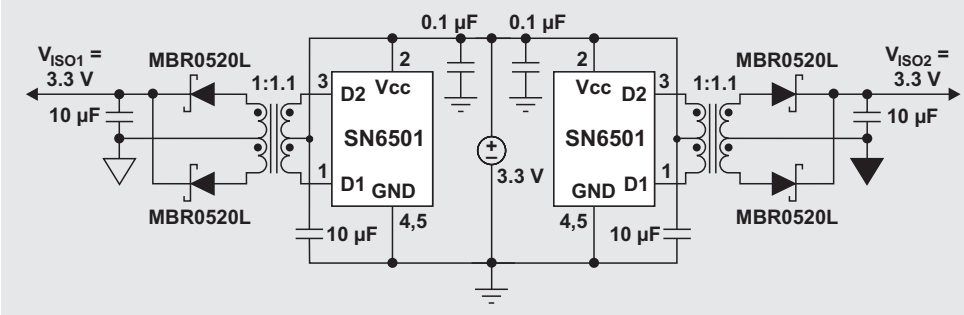

# Using a fixed threshold in ultrasonic distance-ranging automotive applications

**By Arun T. Vemuri**
*Kilby Labs Systems Engineer*

## Introduction

In ultrasonic distance-ranging automotive applications such as ultrasonic park assist (UPA) and blind-spot detection (BSD), ultrasonic waves transmitted by the system are reflected by objects present in the vicinity. The system receives the reflected wave, or echo, and compares the object's echo amplitude against a threshold to detect the object. The echo for objects that are closer to the system is stronger than that for objects that are farther from the system. Hence, it is relatively common for the threshold to be varied with time. This article shows that a variable threshold is not required and that the threshold can remain fixed.

**Figure 1. ADAS using echo processing to detect objects**

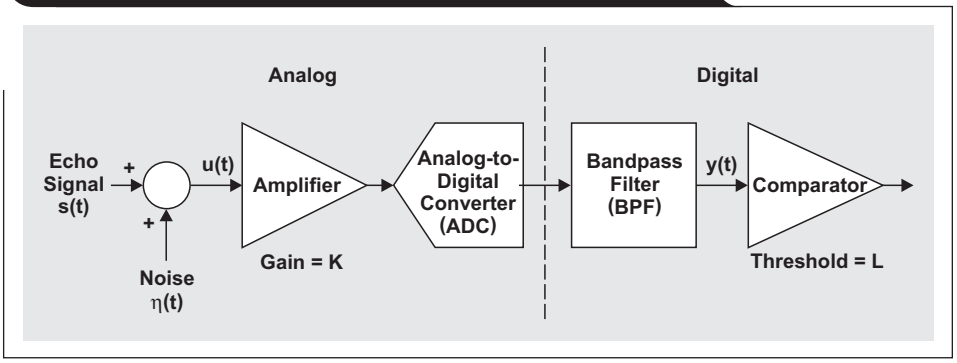


## Ultrasonic distance ranging

One application for ultrasonic distance ranging is an advanced driver-assistance system (ADAS) in a passenger car. Ultrasonic transducers installed in the front and rear bumpers and wing mirrors of an automobile transmit ultrasonic waves and then receive the ultrasonic waves reflected back by nearby objects. An ultrasonic wave's time of flight (TOF) is used to calculate the distance to the objects to assist the driver in parking the car, identifying parking spots, or detecting objects in the driver's blind spot. Up to four transducers are installed in the front and rear bumpers, and one transducer is installed in each wing mirror.

In an ultrasonic ADAS, piezoelectric transducers typically are used to convert electrical signals into ultrasonic waves, and reflected ultrasonic waves into electrical signals. The low receiver sensitivity of piezoelectric ultrasonic transducers usually results in very small electrical signals when the reflected waves are received.

Figure 1 shows a typical signal chain used to process the echo voltage. The Texas Instruments (TI) PGA450-Q1 is an example of an integrated automotive ultrasonic sensor signal conditioner for applications such as UPA systems.

The echo signal, s(t), received by the ultrasonic receiver is corrupted with noise. The input-referred noise, $\eta(t)$, in Figure 1 is the sum of noise from the external environment and all signal-chain components as a function of time (t). This corrupted signal, u(t), is amplified by an amplifier with gain, K, and is digitized with an analog-to-digital converter (ADC). The digitized AM signal is routed through a bandpass filter (BPF), which is primarily used to improve the signal's signal-to-noise ratio. The filtered signal, y(t), is compared against a threshold, L, to detect the presence of an object. BPFs typically are followed by an amplitude demodulator that translates the signal to baseband for comparison. However, for the purpose of this article, the demodulator can be ignored. Thus, the key to detecting the object is the choice of threshold (L). So how does one go about choosing L?

## Echo amplitude

Ultrasonic waves generated by the transmitter are a series of sinusoid pulses at carrier frequency and are characterized by sound pressure level (SPL). The SPL is given by

$$\mathrm{SPL} = 20\log_{10}\left(\frac{p_{rms}}{p_{ref}}\right), \quad (1)$$

where $p_{rms}$ is the RMS sound pressure, and $p_{ref}$ is the reference sound pressure. The commonly used reference sound pressure is 20 µPa, or 0.0002 µbar.

The SPL of ultrasonic waves created by the transducer at an object depends on the object's distance from the transducer. Specifically, the pressure is inversely proportional to the distance:

$$p \propto \frac{1}{d},$$

where p is the pressure of the sound waves, and d is the distance of the object from the transducer. Ultrasonic transducer specifications provide the SPL at 30 cm from the transducer. Given this value, the SPL at arbitrary distance x from the transducer can be calculated by using the distance law,

$$\frac{p_{30\_rms}}{p_{x\_rms}} = \frac{x}{30}, \quad (2)$$

where x is the distance between the transducer and the object, and x > 30 cm. Therefore, the SPL at x is given by

$$SPL_x = SPL_{30} - 20\log_{10}\left(\frac{x}{30}\right).$$

That is, there is loss of sound pressure as the ultrasonic wave travels from the transducer to the object.

The sound waves reflect from the object and return to the transducer, further losing sound pressure. Additionally, due to absorption in air and by the object, the SPL of the received echo can be approximated by Equation 3, shown at the bottom of this page, where $\alpha$ is the absorption coefficient of air. Note that the SPL absorbed in air is proportional to the distance traveled by the sound waves in air. In other words, the SPL loss is proportional to x. A factor of 2 is used because the sound waves travel twice between the transducer and the object—once from the transducer to the object, and once from the object to the transducer.

Based on Equation 1, the sound pressure of the echo pulse received by the transducer can be calculated as

$$p_{echo\_rms} = p_{ref} \times 10^{\frac{SPL_{echo}}{20}}. \quad \textbf{(4)}$$

The ultrasonic receiver converts the received waves into electrical signals. The conversion process is characterized by receiver sensitivity, which is specified in dB. A receiver has 0 dB of receiver sensitivity when it produces 10 V for 1 µPa of sound pressure. Thus, receiver sensitivity specified in dB can be converted to V/µPa by using Equations 5 and 6.

$$RxSensitivity\_dB = 20\log_{10}\left(\frac{\gamma\ V/\mu Pa}{10\ V/\mu Pa}\right), \quad \textbf{(5)}$$

where $\gamma$ is the receiver sensitivity in V/µPa. Equation 5 can be rearranged as

$$\gamma\ V/\mu Pa = 10^{\frac{RxSensitivity\_dB}{20}+1}. \quad \textbf{(6)}$$

**Figure 2. Receiver voltage as a function of the object's distance from the transducer**

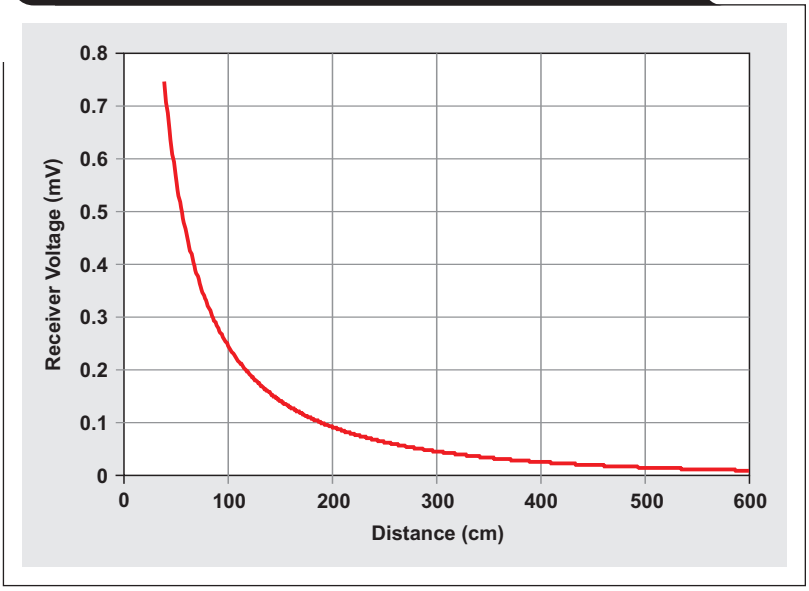


Equations 4, 5, and 6 can be combined into Equation 7, shown at the bottom of this page, to find the voltage produced by the ultrasonic receiver. Equation 7 can be simplified as

$$\gamma_{echo\_rms} = Kp_{ref} \times \frac{30}{2x \times 10^{0.1\alpha x}}, \quad \textbf{(8)}$$

where the gain (K) is a constant.

Equation 8 shows that as the distance x of the object from the transducer increases, the echo voltage decreases. In other words, if the object is closer, the echo amplitude is large, and if the object is farther away, the echo amplitude is small.

Figure 2 shows the received voltage as a function of the object's distance from the transducer, assuming these parameters:

- Transmitted SPL = 106 dB at 30 cm
- Air absorption = 1.3 dB/m
- Object absorption = 0 dB
- Receiver sensitivity = –85 dB

$$SPL_{echo} = SPL_{transmitted} - 20\log_{10}\left(\frac{2x}{30}\right) - 2\alpha x - SPL_{absorbed\ by\ object}, \quad \textbf{(3)}$$

$$\gamma_{echo\_rms} = p_{ref} \times 10^{\frac{SPL_{transmitted} - 20\log_{10}\left(\frac{2x}{30}\right) - 2\alpha x - SPL_{absorbed\ by\ object} + RxSensitivity\_dB}{20}+1} \quad \textbf{(7)}$$

**Figure 3. Demodulated echo-signal waveforms with one possible threshold schedule**

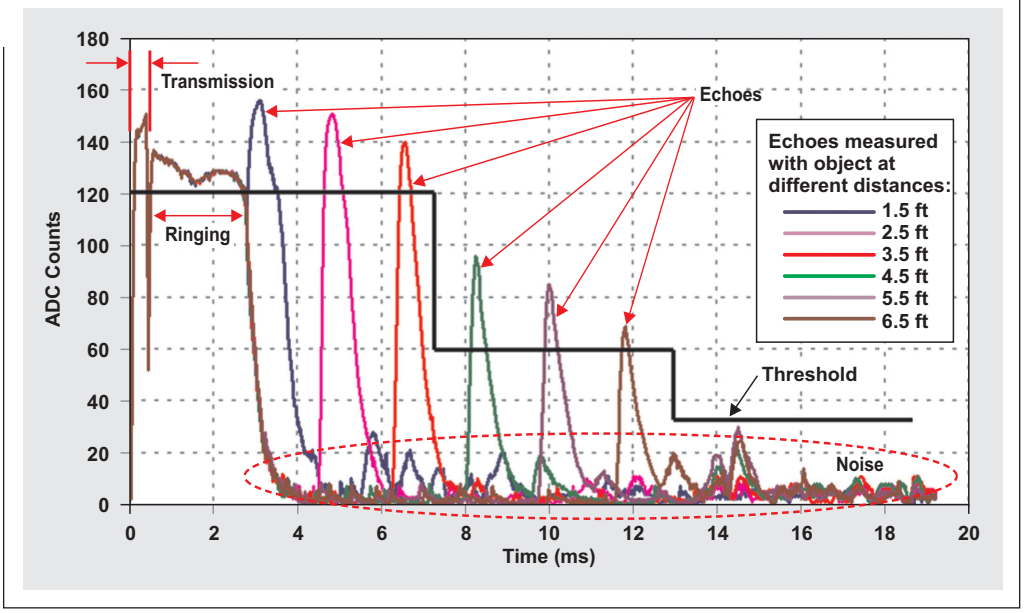


## Variable-threshold scheduling

The previous section showed that the amplitude of the echo received from objects decreases in magnitude as the object's distance from the transducer increases. Further, it is known from Figure 1 that the input signal to the echo-processing path is $u(t) = s(t) + \eta(t)$, where $s(t)$ is the echo signal and $\eta(t)$ is the input-referred noise. In other words, the echo-processing system has to detect the presence of an object by processing the echo signal that not only decreases in amplitude with distance but also is corrupted by noise. One approach normally taken when choosing threshold values is threshold scheduling. In this method, the threshold value is varied with time. Specifically, the threshold value is set to a high value just after the ultrasonic waves are transmitted and is then decreased as elapsed time increases. The rationale behind this approach is to use the predictable decay in signal amplitude to determine the threshold values: The closer the object, the larger are the echo and the threshold for detecting the object. The farther away the object, the smaller are the echo and the threshold.

The concept of the variable threshold is illustrated in Figure 3. This figure shows several sample demodulated echoes for objects at different distances. A test setup with TI's PGA450-Q1 evaluation module was used to collect the waveform data. This figure shows one possible threshold schedule.

While the method of variable-threshold scheduling works in principle, it suffers from two weaknesses:

1. Variable-threshold scheduling requires memory inside the device to store the time-versus-threshold values in the schedule table. If the threshold has 3 possible values as shown in Figure 3, the table will have 6 possible entries. Moreover, for an advanced driver-assistance system (ADAS) in an automobile, customers can store entries for multiple potential installation locations because the transducer can be fitted anywhere on the bumpers or wing mirrors. For example, if the transducer has 10 possible installation locations, up to 60 entries have to be stored in the device. This adds to the device's cost because additional memory is required.
2. System manufacturers "calibrate" the schedule table after installing the transducers in the bumpers and wing mirrors. Calibration is the process of determining the threshold values and times at which the threshold should be switched. The calibration process usually is time-consuming (and hence expensive), especially if multiple entries in the table are needed.

In summary, the main weakness of variable-threshold scheduling is that it increases the overall cost of the ultrasonic ranging system.

## Fixed threshold

In contrast to the variable-threshold approach, which uses time-based threshold values, the fixed-threshold approach uses signal noise as the baseline. The noise in the system is used to determine the threshold so that the absence of objects does not result in detection of objects.

Again, from Figure 1 it is known that the input signal to the echo-processing path is $u(t) = s(t) + \eta(t)$. The echo signal is a series of sinusoid pulses at a carrier frequency, $f_c(t)$, and is given by

$$s(t) = S \times \sin(2\pi f_c t), \quad (9)$$

where S is the amplitude of the echo signal. Therefore,

Equation 10 gives the RMS value of the amplified signal:

$$s_{rms} = \frac{KS}{\sqrt{2}} \quad \textbf{(10)}$$

Note that this series of pulses occurs for only a short duration, making the signal's amplitude appear to be modulated over a long duration of time.

The y(t) output of the bandpass filter (BPF) can be expressed as

$$y(t) = f(\text{BPF}) \rightarrow \left\{ f(\text{ADC}) \rightarrow K\left[ s(t) + \eta(t) \right] \right\}, \quad \textbf{(11)}$$

where $f$(BPF) is the digital-filter function of the BPF and $f$(ADC) is the quantization function of the ADC. Assuming that the reference time for the echo signal is $t_0 = 0$ (which usually is the time at which ultrasonic waves are transmitted by the transmitter), an object is declared to be present at time $t_{object}$ under the conditions $y(t) < L$, $t_{end} < t < t_{object}$, and $y(t_{object}) \geq L$, where $t_{end}$ is greater than zero and is the end of the initial burst of transmitted pulses.

The question is, "Can one choose a fixed threshold instead of using variable-threshold scheduling?" To answer this question, the noise components can be considered by using Equation 12 and assuming that t is an instantaneous value:

$$\eta(t) = \eta_{ext}(t) + \eta_{amp}(t) + \frac{1}{K}\eta_{ADC}(t) + \frac{1}{K}q(t) + \frac{1}{K}\eta_{BPF}(t) \quad \textbf{(12)}$$

The variables are defined as follows:

K = amplifier gain

$\eta_{ext}(t)$ = external noise

$\eta_{amp}(t)$ = amplifier noise

$\eta_{ADC}(t)$ = ADC circuit noise

$q(t)$ = ADC quantization

$\eta_{BPF}(t)$ = mathematical errors in BPF calculations

The individual noise components are independent of each other. Further, it is assumed that each noise component is Gaussian with zero mean and non-zero variance.

When Equations 9 and 12 are substituted into Equation 11, the BPF output becomes

$$\begin{aligned} y(t) &= f(\text{BPF}) \rightarrow \left\{ f(\text{ADC}) \rightarrow K\left[ S \times \sin(2\pi f_c t) + \eta(t) \right] \right\} \\ &= KS \times \sin(2\pi f_c t) + f(\text{BPF}) \rightarrow \left[ K\eta_{ext}(t) + K\eta_{amp}(t) + \eta_{ADC}(t) + q(t) + \eta_{BPF}(t) \right]. \end{aligned} \quad \textbf{(13)}$$

Based on Equation 9, the RMS of the BPF noise is

$$\eta_{rms} = \sqrt{\frac{1}{Q} \times \frac{f_c}{f_s} \times \left[ \left( K\eta_{ext} \right)^2 + \left( K\eta_{amp} \right)^2 + \eta_{ADC}{}^2 + q^2 + \eta_{BPF}{}^2 \right]}, \quad \textbf{(14)}$$

where Q is the quality factor of the BPF, $f_s$ is the ADC sampling frequency, and all noise terms are RMS values.

Given the RMS of noise described by Equation 14, and assuming a 6.6 crest factor, the chosen threshold is

$$L = 6.6\sqrt{\frac{1}{Q} \times \frac{f_c}{f_s} \times \left[ \left( K\eta_{ext} \right)^2 + \left( K\eta_{amp} \right)^2 + \eta_{ADC}{}^2 + q^2 + \eta_{BPF}{}^2 \right]}.$$

The preceding equation can be expressed as

$$L = 6.6K\sqrt{\frac{1}{Q} \times \frac{f_c}{f_s}} \times \sqrt{\eta_{ext}{}^2 + \eta_{amp}{}^2 + \frac{\eta_{ADC}{}^2 + q^2 + \eta_{BPF}{}^2}{K^2}}. \quad \textbf{(15)}$$

In other words, a fixed threshold can be chosen by using Equation 15. Figure 4 shows an example echo response with a fixed threshold.

The obvious advantage of using this method is that it requires only one entry to be stored in memory. If the transducer has the potential to be installed in 10 locations, a total of 10 entries must be stored. This is a sixfold decrease in memory requirements from the variable-threshold method described earlier. Note that Equation 15 also provides a mechanism to scale the threshold, if the amplifier gain (K) is changed.

Equation 15 provides an analytical method to determine the threshold value. Usually, determining the threshold by using noise analysis could be involved. An alternative to performing noise analysis is to calibrate the transducer on the automobile for one threshold. This calibration can be performed by placing the object at the maximum required ranging distance from the transducer. A threshold value can be chosen that is high enough to exceed the noise value of the processed signal when no object is present and that ensures that the signal crosses the threshold only in the presence of an object. Note that when this method is used to choose the threshold, the BPF decay should also be considered. Finally, to increase robustness of object detection, the signal's amplitude must be greater than the fixed threshold for a certain duration.

## Related Web sites

**amplifier.ti.com**
**www.ti.com/product/PGA450-Q1**

**Figure 4. Fixed threshold for echo data**

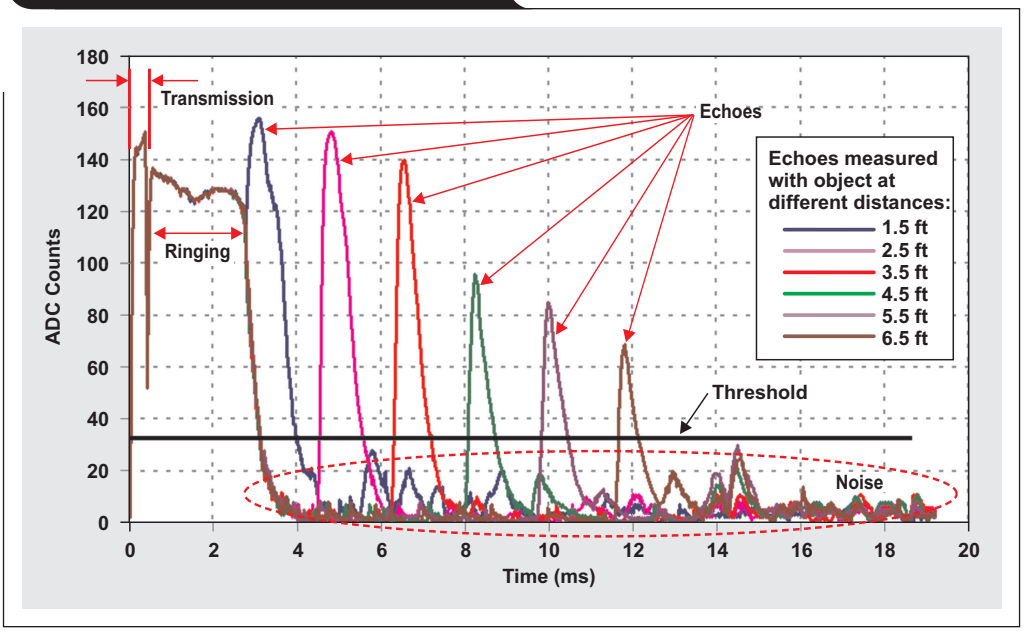

# Applying acceleration and deceleration profiles to bipolar stepper motors

**By Jose I. Quinones**
*Applications Engineer*

## Introduction

With a DC motor, ramping up the voltage (or duty cycle if pulse-width modulation is being used) controls how fast the motor's shaft reaches any given speed. With stepper motors, however, changing the voltage does not have any effect on the motor speed. While it is true that changing the voltage changes the rate of current charge across the windings and thus the maximum speed the stepper can reach, the motor speed is set by the rate at which the current through the windings is switched, or commutated.

Can it be assumed that steppers are machines not requiring controlled acceleration profiles? If so, can steppers be run at any target speed desired without consequences? The truth is that stepper-motor motion needs to be actuated through acceleration and deceleration profiles more than any other motor topology. Trying to start at any speed may have dire effects.

In this article it is assumed that the reader is well-versed in how a commercially available integrated microstepping driver is used to control a stepper motor. The output of a stepper driver, such as the Texas Instruments (TI) DRV8818, is directly proportional to the frequency of a square wave (STEP input). Each STEP pulse equals a step (or microstep) as defined by the driver's stepping logic. Hence, changing the frequency of the square wave also changes the stepper's rate accordingly.

Figure 1 shows a motor manufacturer's conventional stepping rate/torque curve with an important parameter, $f_s$, called the starting frequency. It must be understood that, for this particular motor to start properly, a stepping rate smaller than $f_s$ must be employed. To start the motor with a stepping rate larger than $f_s$ may induce the motor to stall and lose synchronization. Once this happens, motion control is severely compromised. This appears to be a major problem but actually can be solved quite easily. All that is needed is to start the motor at a stepping rate below $f_s$ and then increase the speed until the target speed is reached. Following this guideline, the stepper motor can be actuated with stepping rates far exceeding $f_s$—as long as the speed is kept below the shown torque/speed curve.

Equally important, one should not attempt to stop the motor simply by halting the STEP pulses. Instead, the stepping rate should be decreased from the target speed to a lower rate at which the motor can stop without the shaft inertia inducing extra and unwanted steps. Remember that if the stepper is being utilized in a positioning application, the motor shaft can lose position if it keeps on moving after it should have stopped. Since closed-loop position

**Figure 1. Torque/speed curve for a bipolar constant-current stepper motor**

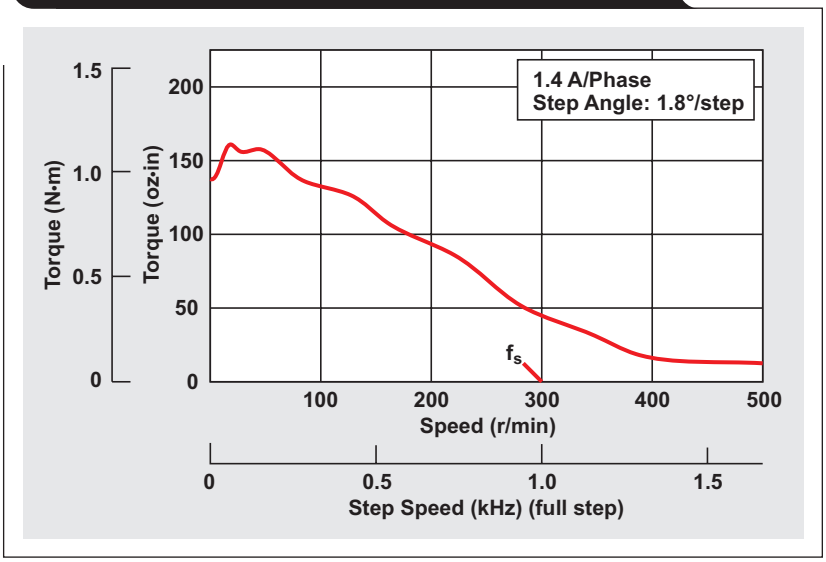

feedback is seldom used for driving steppers, it is crucial to ensure that only the commanded steps take place.

## Acceleration/deceleration profile

To accelerate a stepper from a starting speed to a desired target speed, the current speed just needs to be changed at periodic intervals. Most engineers use microcontrollers to achieve stepper control. The most common implementation uses only two timers. The first is a steps-per-second (SPS) timer used to generate an accurate timing function for the stepping rate. The second is an acceleration timer used to alter the first timer on a periodic basis. Since the speed is being changed at timely intervals, in essence the angular velocity with respect to time (dv/dt) is being derived. This derivation is called acceleration, or how speed changes across time. Figure 2 shows an enlarged view of a typical microcontroller-based acceleration profile and what is happening as the stepper is accelerated towards a target speed.

The SPS is the desired number of steps per second, or the stepping rate, at which the motor should move. The SPS timer must be programmed to issue pulses at this rate. Depending on the timer's oscillator frequency, a typical equation is

$$\text{SPS\_timer\_register} = \frac{\text{timer\_oscillator}}{\text{SPS}},$$

where SPS_timer_register is a 16-bit number that tells the timer how long it takes to generate subsequent STEP pulses, and timer_oscillator is a constant of how fast the timer is running in megahertz.

This equation is stored in a function because it is used quite frequently. To see how it works, assume that the timer oscillator is running at 8 MHz and the desired stepping rate for the motor is 200 SPS. According to the equation, the program code makes the value of SPS_timer_register equal to 40,000. So every 40,000 timer clicks, a STEP pulse is generated. This results in a timer-based output of 200 pulses per second and a shaft rotation equal to 200 SPS.

Every time such an event takes place, an interrupt is generated and the timer is cleared. The timing of the rising edge at the STEP input is crucial to the microstepping driver's accuracy, but the falling edge can happen at almost any time as long as it is well before the next STEP rising edge.

Two parameters are needed to define the acceleration curve: (1) how often to change the SPS value, and (2) by how much. The acceleration curve is directly proportional to both parameters; that is, the more often the SPS value is updated and the higher its value, the steeper will be the acceleration curve. The acceleration timer handles both parameters: The timer function fires as many times per second as is desired to change the SPS value, and the timer's interrupt-service routine (ISR) determines what the new speed is by incrementing the current SPS by a predetermined factor.

The acceleration rate is measured in steps per second per second (SPSPS), or by how many times per second the current SPS rate is changed. If the SPS value is changed by adding a one, the acceleration timer's ISR must be called (triggered) for each change in the acceleration rate. For example, with an acceleration rate of 1000 SPSPS, the motor speed can be started at 200 SPS and incremented by one until it reaches 1200 SPS. The acceleration timer's ISR would then need to be called 1000 times.

Another option is to call the acceleration timer half as frequently and then increment the SPS by two. Compared to the previous example, the acceleration timer's ISR is called only 500 times, but the motor still starts up at 200 SPS and reaches 1200 SPS within a second. The difference is more real-time availability at the expense of resolution. In other words, to achieve an accurate acceleration rate of 999 SPSPS, the first option must be used.

**Figure 2. Close-up of a typical acceleration profile**

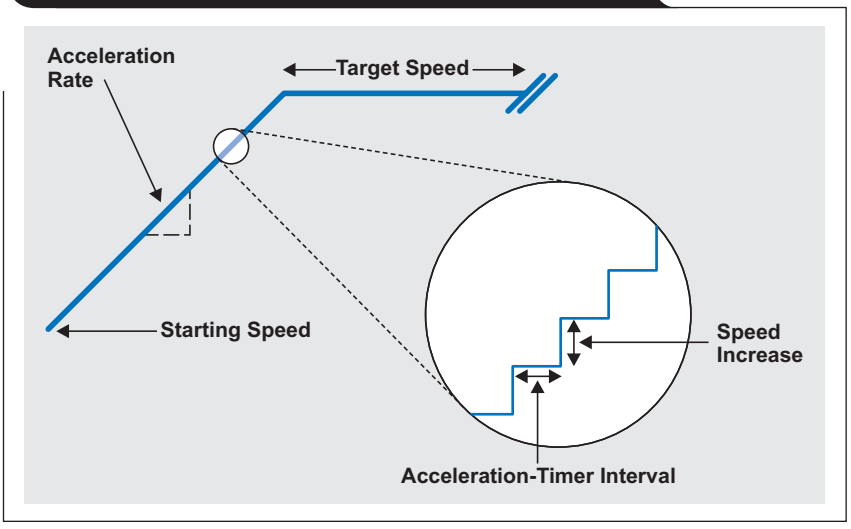

**Figure 3. Acceleration/deceleration profile**

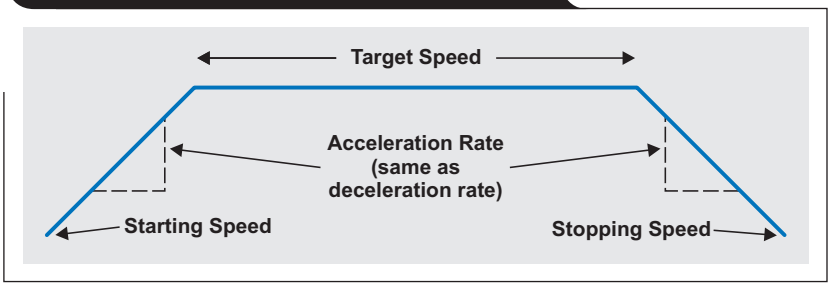


The trade-offs of choosing one option versus the other must not be ignored, as the choice defines what kind of motion quality can be obtained. For instance, if a lot of granularity is required in order to achieve every possible acceleration profile, the acceleration timer's ISR will need to be called as much as possible.

However, in the SPS-timer equation given earlier, there is a division operation. Depending on which processor core is being employed, this division may considerably limit how many times the ISR can effectively be called and still correctly generate the new SPS rate. In an implementation using TI's MSP430™ with the CPU running at 16 MHz, a division operation takes about 500 µs. As a result, the most the ISR can be called per second is 2000 times. This limit then defines the incrementing factor. For any acceleration rate larger than 2000, an increment larger than one must be used.

The acceleration rate is computed once, shortly before the motor is started. The software in charge of this computation determines what the acceleration timer's interval and increment factor will be, then configures the variables accordingly. These variables are used concurrently until the SPS rate is modified enough to reach the target speed. Once the target speed is met, the acceleration profile ends.

The deceleration profile is basically identical to the acceleration profile, except that the increment factor is negative rather than positive. Also, a new target speed must be specified at which the motor can be safely stopped. Figure 3 shows an acceleration/deceleration profile where the acceleration and deceleration rates are symmetric. Asymmetric rates can also be employed.

## Position control

Up to this point, operating the motor in a speed-control loop has seemed fairly simple. The motor is brought into a target speed and at some point commanded to stop. However, what happens when a predetermined number of steps needs to be executed in a predetermined amount of time? The acceleration/deceleration profiles then become more important than ever. In this motion-control topology, it is crucial that the motor stop when all the programmed steps have been executed. The variable that specifies how many steps will be issued is called number_of_steps.

The motion profile must be coded to make the motor stop at the required time rather than wait for a command to start deceleration. One way to achieve this is to program a variable called steps_to_stop to be smaller than number_of_steps. The software then determines when deceleration needs to be engaged by monitoring steps_to_stop.

Acceleration will not complete execution until the target speed has been reached. Once this happens, the stepper is allowed to run until it reaches the steps_to_stop count, at which time deceleration begins. For example, for a 1000-step run, steps_to_stop is set to 800. Hence, the motor is started via an acceleration profile and runs until step 800 is reached, at which time the motor decelerates until it stops.

Depending on how all of the system's variables are configured, five important scenarios need to be examined (see Figure 4).

**Scenario 1:** All steps are issued before the motor reaches the target speed.

**Scenario 2:** All steps are issued while the motor is at the target speed.

**Scenario 3:** All steps are issued before the stopping speed is reached.

**Scenario 4:** All steps are issued as the stopping speed is reached.

**Scenario 5:** All steps are issued after the stopping speed is reached.

Stopping the motor right as the stopping speed is reached (Scenario 4) is the ideal case. Stopping the motor shortly before the stopping speed is reached (Scenario 3) or after it is reached (Scenario 5) can be acceptable depending on how many steps away from the ideal case these events occur. For instance, if all steps are issued while the motor is moving too fast, the motor shaft may lose position due to rotor inertia. But if the stopping speed is reached before all the steps are executed, the total time needed to execute the profile can become too long.

Scenarios 1 and 2, portrayed for illustrative purposes only, should not take place, as the designer should always ensure that steps_to_stop is smaller than number_of_steps. Knowing all the possible scenarios, the designer can easily tune the system to acquire the optimal response.

**Figure 4. Five acceleration/deceleration scenarios**

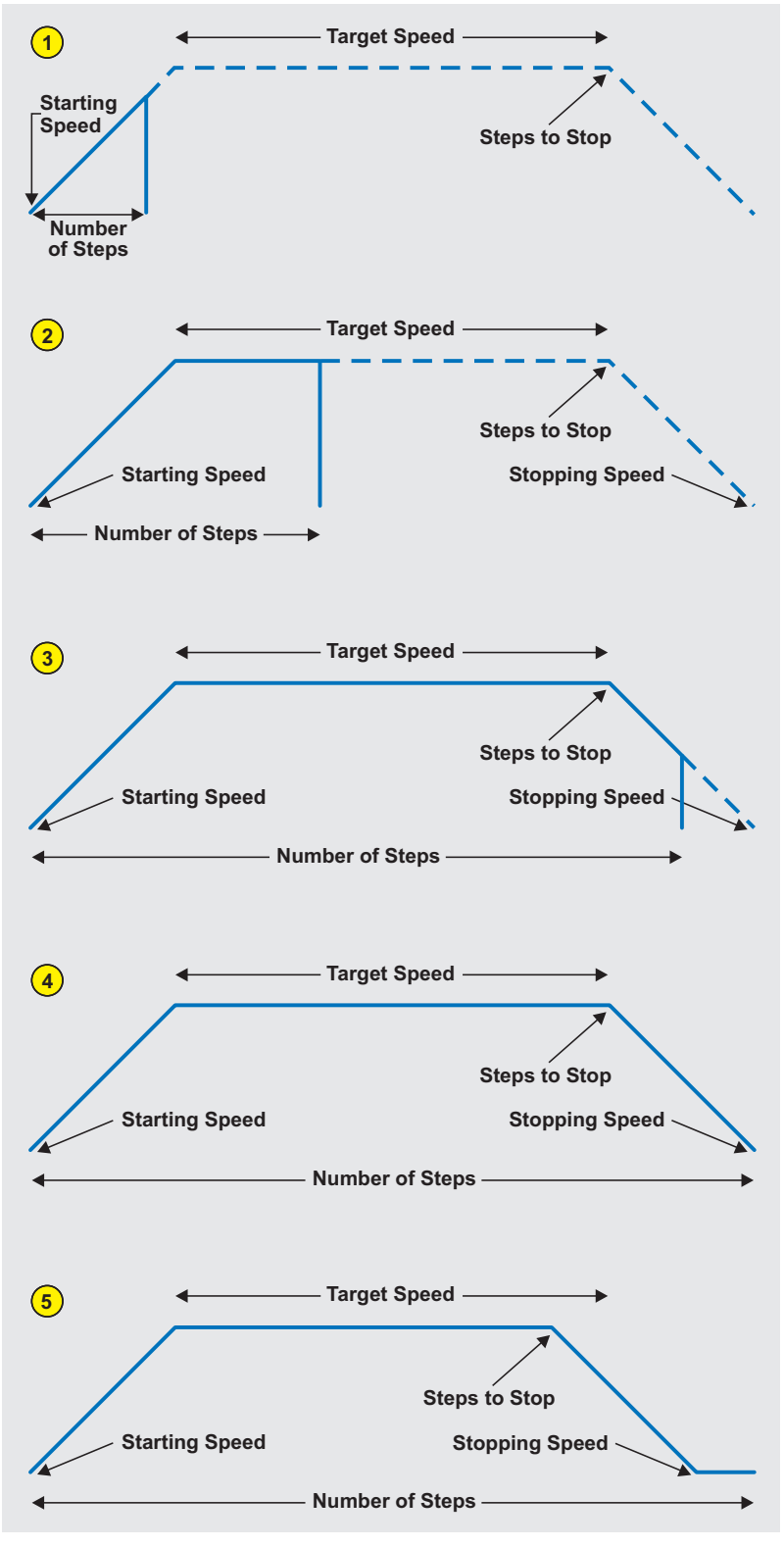

Another option that may result in less tuning is to segment the total number of steps into percentages assigned to each particular region of the acceleration/deceleration profile. In this algorithm implementation, 20% of the total number of steps can be selected to accelerate the motor, 60% to run the motor at a constant (reached) speed, and the remaining 20% to decelerate the motor (see Figure 5). If number_of_steps is 1000, the stepper accelerates at the programmed acceleration rate for 200 steps and stops acceleration at whatever step rate it reaches. It then executes 600 steps at this rate, with the last 200 steps being executed throughout the deceleration profile.

**Figure 5. Acceleration/deceleration profile based on percentages**

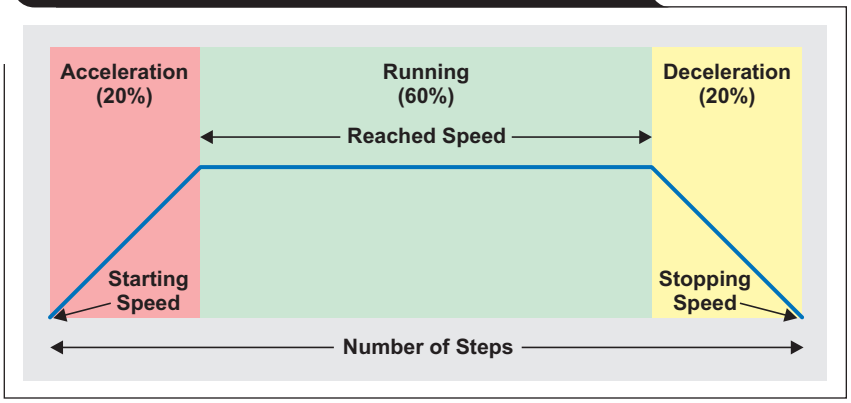


Notice that with an algorithm of this nature, assuming that the percentages are selected correctly, it is impossible to run out of steps on the wrong portion of the motion profile. For the example in Figure 5, since both the acceleration and deceleration portions are balanced, the motor most likely starts and stops at the same speed. The disadvantage of this method is that it is very hard to ensure what the target speed will be. If the target speed is not important, then this algorithm can be used to ensure that the motor will always stop at a safe speed.

If the speed reached is too slow for the application, the only means to speed up the motor shaft with this algorithm is to increase the acceleration rate or increase the percentages of the number of steps used in the acceleration/deceleration regions. However, the designer must be careful not to take the motor into a speed that violates the motor's torque/speed curve.

## Conclusion

Accelerating and decelerating a bipolar stepper motor is a crucial part of designing any application that uses one. While power-stage control has been simplified considerably throughout the last decade, the application of acceleration and deceleration profiles still resides in the realm of the application's processor. Because of the wide availability of stepper solutions, the algorithms to process proper motion control for the application's stepper motor are easier to code and tune. By accelerating and decelerating the motor properly, the designer ensures that the application will operate efficiently and according to specifications.

Please see Reference 1 for more information about the code structure for an acceleration/deceleration-based implementation that revolves around a power stage similar to the DRV8818 and uses an MSP430 microcontroller.

## Reference

For more information related to this article, you can download an Acrobat® Reader® file at www.ti.com/lit/*litnumber* and replace "*litnumber*" with the **TI Lit. #** for the materials listed below.


| **Document Title** | **TI Lit. #** |
|---|---|
| 1. Jose Quinones, "Intelligent stepper motor driver with DRV8811/18/24/25," Application Report. . . . . | SLVA488 |


## Related Web sites

**www.ti.com/motor**
**www.ti.com/product/***partnumber*
Replace *partnumber* with DRV8811, DRV8818, DRV8824, or DRV8825

# High-definition haptics: Feel the difference!

**By ShreHarsha Rao**
*Product Line Manager, Haptics*

While most smartphone and tablet users already have experienced haptics, the term itself is mostly unknown to consumers. In its basic definition, "haptics" refers to the science of tactile feedback. The most basic form of haptics is when a cell phone vibrates, indicating either an incoming call or the arrival of a message in the phone's inbox. In these cases, the user's attention is grabbed by a tactile alert.

About one-third of smartphones include tactile feedback that extends beyond a vibration alert. A common example is the subtle vibrations a user feels when typing an email or texting. Each vibration confirms that a keystroke has registered. Users tend to commit fewer typing errors and have a more satisfactory experience when tactile feedback exists.

## Enhancing the user experience with haptics

More and more mobile devices such as cell phones and tablets are now touch-enabled. Touch interface is so intuitive that toddlers can unlock a smartphone and click on the YouTube icon to view the playlist. However, touch screens have one major limitation in that there is no physical or mechanical feedback for user interactions or alerts. Well-designed haptics can significantly enhance the overall user experience of a touch-enabled mobile device.

Haptics has more usage than just serving as an alert or typing confirmation. Standard gestures like swipe to unlock, pinch to zoom, and push/pull to scroll could have their own haptic/tactile signatures. The feedback could increase as the user zooms in to the maximum enlargement of the view. Faster scrolling could provide faster tactile feedback. If this kind of context-sensitive feedback were combined with audiovisual feedback, the resulting consumer experience would be highly satisfactory and intuitive.

Haptics also brings in an element of fun. Many people play games on their mobile devices. Tactile feedback can be used to make the gaming experience significantly better. For example, in a first-person shooter game, the shooter could actually feel the weapons being fired. The user could feel crashes and bumps in a racing game, feel tension when releasing the string in the popular Angry Birds game, feel the guitar strings or piano keys, and so on. The possibilities are as endless as the game developer's imagination!

## Inertial haptic actuators (ERMs/LRAs)

The standard haptics in a cell phone is due to a small motor called the eccentric rotating mass actuator (ERM). As the motor is driven with a voltage and starts to spin, a vibration is felt. A haptic driver chip drives this motor differentially, so the motor spins when a positive voltage is applied and brakes when reverse polarity, or a negative voltage, is applied. This works perfectly for vibration alerts. However, trying to use an ERM for other haptic applications, like gaming, quickly runs down the battery.

The ERM is inertial and needs overdrive to spin faster. Start-up time, defined as the time it takes for the motor to reach 90% of the rated acceleration, is usually in the range of 50 to 100 ms. Braking or stopping the motor involves a similar time frame. For a very simple haptic event like a click, the overhead is about 100 to 200 ms. If the application demands repeated haptic events, the latency associated with motor-based haptics may be undesirable.

Another aspect of the ERM is the buzzing or audible noise associated with the spinning motor. This is less of a concern if the haptic feedback is combined with audio feedback. However, in a silent conference room, everyone can hear the motor as someone types a message. The ERM also has few discernible haptic effects that can be generated by the user. The vibration frequency and amplitude are tied to a single control voltage.

Another type of inertial actuator, the linear resonant actuator (LRA), is used in some smartphones for haptics and vibration alerts. The LRA is of a different mechanical construction than the ERM. It consists of spring-mounted mass and vibrates in a linear motion. The LRA must be driven at a narrow resonant frequency. It also tends to have a slightly better start-up time than the ERM.

Depending on the manufacturer, start-up time varies from 40 to 60 ms (Figure 1). This offers a slight improvement over the ERM start-up time of between 50 and 100 ms. By modulating the resonance-carrier amplitude, it is possible to produce a variety of different haptic effects.

**Figure 1. Typical start-up time of an LRA is 40 to 60 ms**

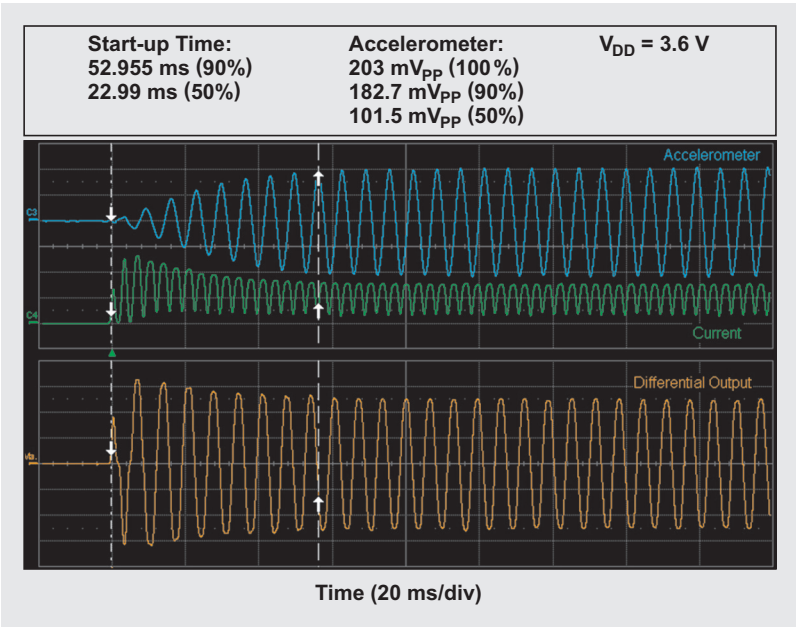


## High-definition haptics

Just as high-definition (HD) TV offers higher resolutions than standard-definition TV to create a sharper and more discernible image, HD haptics lets users feel more discernible vibration effects than the buzz of inertial actuators. Piezoelectric (piezo) or ceramic haptic actuators are used to implement HD haptics and offer compelling differences from ERMs/LRAs).

### Piezo actuators

When differential voltage is applied across both ends of a piezo actuator, it bends or deforms, generating a vibration. Piezo actuators need high voltage to deform. Depending on the manufacturer, voltage can vary from 50 to 150 $V_{PP}$. At higher voltages, the number of required piezo layers decreases; so at 150 $V_{PP}$ the piezo actuator has approximately 4 layers, whereas at 50 $V_{PP}$ there may be as many as 16 to 24 layers. At higher voltages, due to the reduced number of layers, the piezo actuator's capacitance is lower. In other words, less current is needed to drive lower-capacitance haptic actuators.

Piezo actuators are available as disks or as rectangular strips, also called benders. Piezo disks deform vertically and can be used for z-axis vibration. Piezo benders can be mounted directly to a "floating" touch screen to vibrate only the screen (Figure 2a). Piezo benders can also be mass mounted in a small module that can be mounted to the device's case or PCB to provide vibration for the whole device (Figure 2b). Piezo modules have become popular because mechanical integration is easy.

**Figure 2. Form factors for piezo actuators**

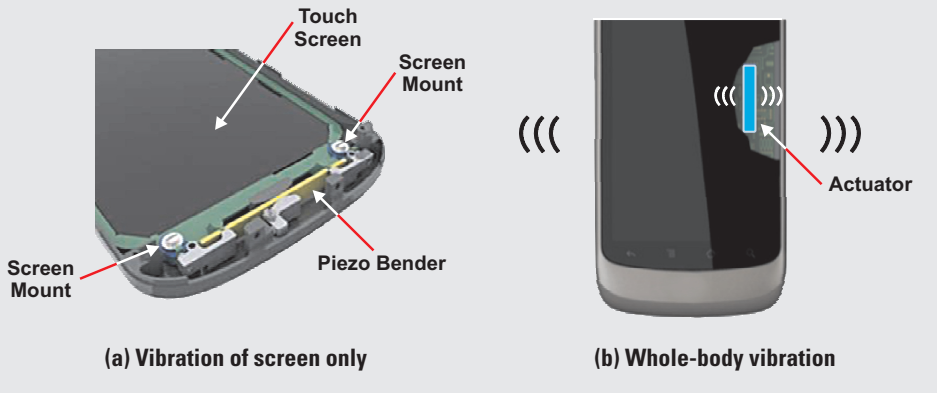

### What makes piezo actuators HD?

Four key elements differentiate piezo actuators from inertial actuators:

1. *Faster start-up time:* Due to inherent mechanical properties of piezo actuators, start-up time is very fast—typically less than 15 ms, which is three to four times faster than ERMs. Compared to ERMs, the duration of the overall haptic event may be shortened by 70 ms. This is further illustrated in Figure 3.
2. *Higher bandwidth:* The higher bandwidth of piezo actuators, illustrated in Figure 4, provides a more detailed haptic palette with a greater number of effects.
3. *Lower audible noise:* Unlike ERMs, piezo actuators have no spinning mass to create mechanical noise.

**Figure 3. Typical start-up time of a piezo module is ~14 ms**

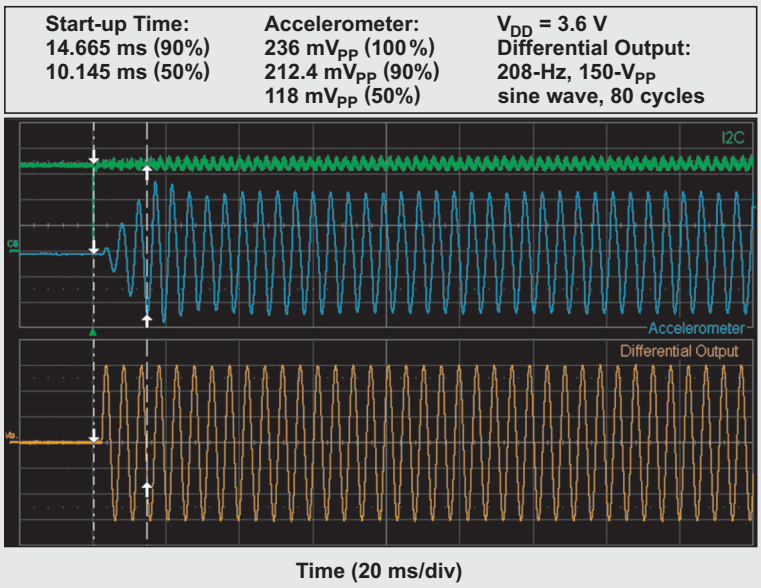


**Figure 4. Higher bandwidth of piezo actuators (ideal model)**

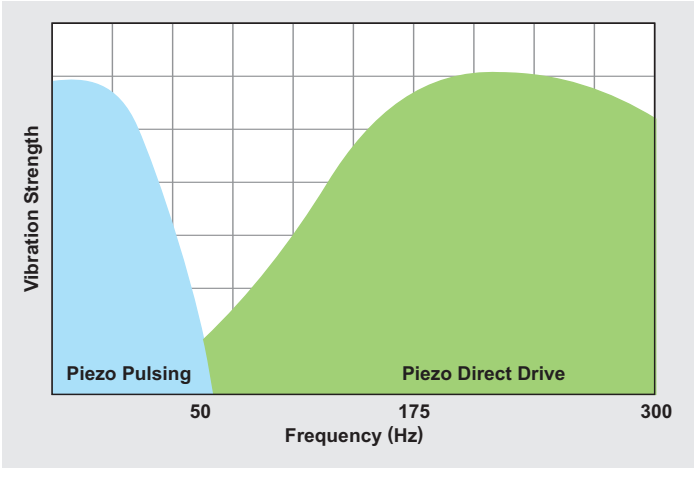

4. *Stronger vibration:* Piezo modules tend to generate higher vibration strengths. Figure 5 shows the acceleration characteristics of a commercially available piezo module, and Figure 6 shows the acceleration characteristics of a commercially available LRA. It can be seen that the piezo actuator generated a peak-to-peak acceleration of 3 $G_{PP}$, compared to less than 1.5 $G_{PP}$ in the case of the LRA. This higher vibration strength implies that piezo modules are a great candidate for bigger-screen smartphones and tablets.

### Current consumption of piezo actuators

Even though piezo actuators need higher voltage than standard inertial actuators, the actual current consumption is lower than that of ERMs and on a par with that of LRAs (see Table 1).

## Conclusion

Piezo actuators deliver significant performance and cost advantages compared to inertial actuators. Their faster start-up time helps create sharp and crisp clicks for keyboard applications. Their higher bandwidth helps create more user-perceivable haptic effects that are critical for gaming applications. The stronger vibration strength of piezo actuators can be used to generate haptic feedback for bigger consumer devices like tablets and e-readers. Overall, piezo haptics offers compelling features to enhance the tactile feedback experience and helps improve the overall user experience of mobile devices.

Texas Instruments (TI) offers both analog-input (DRV8662) and digital-input (DRV2665) piezo haptic drivers that interface with a wide variety of piezo actuators on the market. TI also has demos that let designers "feel the difference."

## Related Web sites

**www.ti.com/haptics-ca**
**www.ti.com/product/DRV2665**
**www.ti.com/product/DRV8662**

**Figure 5. Acceleration characteristics of a piezo module**

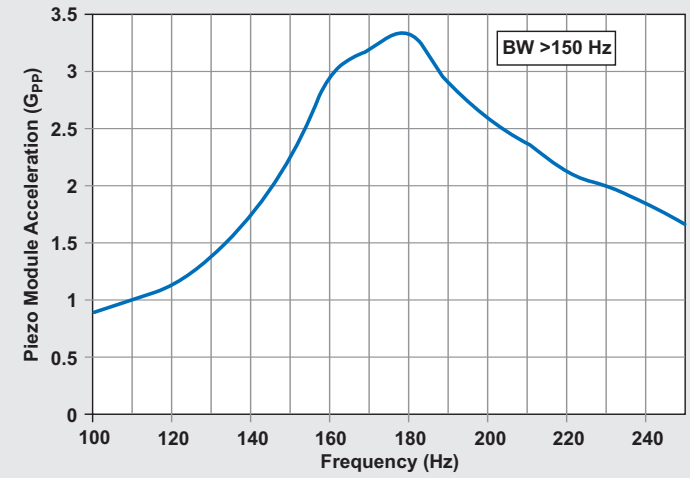


**Figure 6. Acceleration characteristics of an LRA**

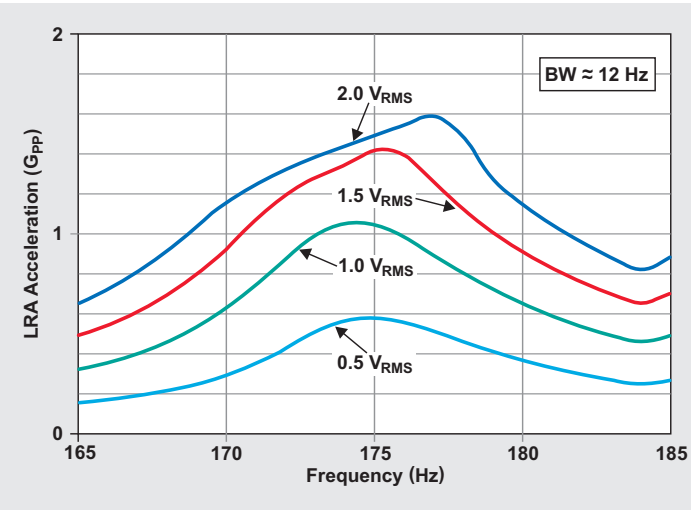


**Table 1. Power consumption of haptic actuators**

| USAGE | PIEZO ACTUATOR (mAh) | LRA (mAh) | ERM (mAh) |
|---|---|---|---|
| Per 25 phone calls | 2.685 | 1.497 | 3.540 |
| Per 50 text messages | 25.660 | 11.869 | 27.480 |
| Per 4 hours of e-mail access | 28.076 | 12.150 | 29.078 |
| Crossword game (60 min) | 1.094 | 0.487 | 1.150 |
| DoodleJump game (30 min) | 6.270 | 3.975 | 8.170 |
| Shooting game (30 min) | 24.976 | 37.777 | 61.558 |
| Total power | 88.761 | 67.755 | 130.975 |
| Discharge percentage of 1200-mAh battery | 7.4% | 5.6% | 10.9% |

# Index of Articles

## Power Management *(Continued)*

# TI Worldwide Technical Support

## Internet

### TI Semiconductor Product Information Center Home Page
support.ti.com

### TI E2E™ Community Home Page
e2e.ti.com

## Product Information Centers

**Americas** Phone +1(972) 644-5580

**Brazil** Phone 0800-891-2616

**Mexico** Phone 0800-670-7544

Fax +1(972) 927-6377
Internet/Email support.ti.com/sc/pic/americas.htm

### Europe, Middle East, and Africa

Phone
European Free Call 00800-ASK-TEXAS (00800 275 83927)
International +49 (0) 8161 80 2121
Russian Support +7 (4) 95 98 10 701

**Note:** The European Free Call (Toll Free) number is not active in all countries. If you have technical difficulty calling the free call number, please use the international number above.

Fax +(49) (0) 8161 80 2045
Internet www.ti.com/asktexas
Direct Email asktexas@ti.com

### Japan

Phone Domestic 0120-92-3326
Fax International +81-3-3344-5317
Domestic 0120-81-0036
Internet/Email International support.ti.com/sc/pic/japan.htm
Domestic www.tij.co.jp/pic

### Asia

Phone
International +91-80-41381665
Domestic Toll-Free Number

**Note:** Toll-free numbers do not support mobile and IP phones.

Australia 1-800-999-084
China 800-820-8682
Hong Kong 800-96-5941
India 1-800-425-7888
Indonesia 001-803-8861-1006
Korea 080-551-2804
Malaysia 1-800-80-3973
New Zealand 0800-446-934
Philippines 1-800-765-7404
Singapore 800-886-1028
Taiwan 0800-006800
Thailand 001-800-886-0010

Fax +8621-23073686
Email tiasia@ti.com or ti-china@ti.com
Internet support.ti.com/sc/pic/asia.htm



**A011012**



**SLYT477**